An Investigation into the Combustion and Performance of Small Solid-Propellant Rocket Motors

Morgan G. Carter[1]

University of New South Wales (UNSW) at the Australian Defence Force Academy (ADFA)

This thesis project involved producing a thrust-measuring instrument to accurately measure the thrust-time profiles, hence impulses, of small solid-propellant (black-powder or gunpowder) rocket motors manufactured by a company called *Estes Industries*. These measured profiles were compared with the accepted thrust-time profiles and impulses provided in the Estes product catalogue. A temperature sensitivity analysis of motor performance was also conducted to determine how initial propellant temperature affects the thrust-time profiles of the Estes solid-propellant rocket motors. Amateur model rocket enthusiasts could potentially store then launch their small, black-powder rocket motors in locations here on Earth that could be at temperatures in the range of -30°C to +50°C. It is therefore useful for them to know how the propellant temperature will affect the performance of their rocket motors. This sort of analysis also has many military applications. High-performance military solid-propellant missiles/rockets could be launched after storage periods at temperatures within a similar range. The storage temperature of the missiles/rockets will affect their trajectories during operation. Results from this experimentation have been qualified using rocket theory and quantified using calculations. The temperature sensitivity of the black-powder propellant used in the Estes motors has been compared with typical values for other commercially-manufactured motors. Once the thrust-time-temperature relationships of the black-powder Estes rocket motors were determined and interpreted, this thesis project culminated with the design, construction and testing of two home-made solid-propellant rocket motors. This thesis succeeded in creating home-made motors that represent a cheaper alternative to the motors produced commercially, such as the Estes motors; however, more development work is required to match the performance of the home-made motors with the Estes products. This thesis contains the necessary depth of knowledge to produce a home-made solid-propellant rocket motor safely, while providing a general insight into the engineering involved in solid-propellant rocketry.

[1] Sub Lieutenant, RAN, School of Aerospace, Civil & Mechanical Engineering (SACME). Aeronautical Engineering: Project, Thesis and Practical Experience ZACM 4049/4050.

Contents

Contents **2**
Nomenclature **3**
I. Introduction **4**
II. Background Theory **4**
A. Introduction to Solid-Propellant Rocket Motors 4
B. Rocket Propulsion Principles 5
1. Impulse and Mass Fraction *6*
2. Thrust *6*
C. Solid Propellant 7
D. Temperature Sensitivity of Solid-Propellant Grains 8
E. Rocket Performance Testing 9
F. Instrumentation and Measurement 10
III. Phase One — Confirming the Thrust-Time Profiles of the Estes Motors **11**
A. The Thrust-Measuring Instrument 11
1. Design of the Thrust-Measuring Instrument *11*
2. Mock-Up Instrument Trial *12*
3. Refined Instrument *13*
4. Experiment Setup *13*
5. Obtaining the Thrust-Time Profiles *15*
B. Comparison of Measured Motor Performance with Estes-Claimed Motor Performance 16
1. Collection and Presentation of the Measured Results *16*
2. Analysis and Comparison of Motor Performance Results *18*
IV. Phase Two — Determining the Temperature Sensitivity of Estes Motor Performance **21**
A. Temperature Sensitivity Experiment Method 21
1. Selecting the Storage Temperatures *21*
2. Storage Time Period *22*
3. Firing the Rocket Motors *23*
4. Thrust-Measuring Instrument Design Flaw *23*
B. Analysis of Temperature Sensitivity Results 24
1. Collection and Presentation of Measured Results *24*
2. Analysis of the Results *26*
V. Phase Three — Designing, Constructing & Testing Home-Made Solid-Propellant Motors **27**
A. Designing the Home-Made Motors 27
1. The Home-Made Propellant Recipe *27*
2. Designing the Motor Cases, Nozzles and End-Caps *28*
B. Construction of the Home-Made Motors 29
1. Constructing the Motor Cases, Nozzles and End-Caps *29*
2. Constructing the Home-Made Ignition System *29*
3. Packing the Motor Cases with Propellant *30*
C. Testing the Home-Made Rocket Motors 30
1. Experiment Setup *30*
2. Measured Performance of the Home-Made Motors *30*
3. Analysis of Measured Results *32*
VI. Conclusions **33**
VII. Recommendations **33**
Acknowledgements **33**
References **34**

APPENDICES (In supplementary documents)
Appendix A. Analysis of Cantilever Beam A1
Appendix B. Rigid Cantilever Beam Analysis Spreadsheet B1
Appendix C. Analysis of Wheel and Pendulum Design C1
Appendix D. MATLAB Demonstration of Wheel Instrument Design D1
Appendix E. Analysis of Pressure Instrument Design E1
Appendix F. Analysis of Hinged-Cantilever Beam Design F1
Appendix G. Section III, Part G, Initial Thesis Report G1
Appendix H. Section III, Part H, Initial Thesis Report H1
Appendix I. Thrust-Measuring Instrument Drawings I1
Appendix J. Thrust-Measuring Instrument Calibration Data J1
Appendix K. Phase One Measured Results and Data K1

Appendix L.	Phase One Results Analysis and Comparison	L1
Appendix M.	Room Temperature Records	M1
Appendix N.	Phase Two Measured Results and Data	N1
Appendix O.	Rocket Design Process, Calculations and MATLAB Code	O1
Appendix P.	Home-Made Motor Drawings	P1
Appendix Q.	Phase Three Measured Results and Data	Q1
Appendix R.	Project Costing	R1
Appendix S.	Client Brief	S1
Appendix T.	Milestone Chart	T1
Appendix U.	Phase One Risk Assessment	U1
Appendix V.	Phase Two Risk Assessment	V1
Appendix W.	Phase Three Risk Assessment	W1
Appendix X.	Phase Three Chemical Risk Assessment	X1
Appendix Y.	Chemical Issues Form	Y1

Nomenclature

I_t	=	total impulse [N s]
F	=	thrust force [N]
t_b	=	burning time of propellant grain [s]
I_s	=	specific impulse [s]
$\dot{m}$	=	propellant mass flow rate [kg s^{-1}]
g_0	=	acceleration due to gravity [m s^{-2}]
c	=	effective exhaust velocity [m s^{-1}]
ζ	=	propellant mass fraction
m_p	=	propellant mass [kg]
m_0	=	vehicle/motor initial mass [kg]
v_2	=	instantaneous exhaust velocity [m s^{-1}]
F_T	=	total thrust [N]
p_2	=	exhaust gas pressure at the nozzle exit [Pa]
p_3	=	ambient fluid pressure [Pa]
A_2	=	nozzle exit area [m^2]
d_2	=	nozzle exit diameter [m]
A_t	=	nozzle throat area [m^2]
d_t	=	nozzle throat diameter [m]
r	=	propellant burn rate [m s^{-1}]
a	=	empirically determined constant of burn rate
n	=	empirically determined constant of burn rate
p *or* p_1	=	combustion-chamber pressure [Pa]
A_b	=	burning area of propellant grain [m^2]
ρ_b	=	propellant density [kg m^{-3}]
σ_p	=	temperature sensitivity of burning rate at constant pressure [K^{-1}]
T_0	=	propellant initial temperature [K]
π_K	=	temperature sensitivity of pressure at constant motor geometry [% $°C^{-1}$]
K	=	ratio of propellant burning area to nozzle throat area
R	=	linear correlation or linearity
m_f	=	vehicle/motor final mass [kg]
$f(t)$	=	scaled thrust data at time, t [s], obtained using DAQ system [g]
$F(t)$	=	adjusted scaled thrust data at time, t, in [N]
C	=	thrust-zeroing adjustment constant [N]
$\Delta t_{correction}$	=	time alignment correction value [s]
$\bar{y}$	=	sample mean
μ	=	population mean
s	=	sample standard deviation
σ	=	population standard deviation
N	=	number of motors in a sample
y_i	=	value for a particular profile feature for the i^{th} motor in the sample
b	=	number of D11-P motors in each temperature batch
L_b	=	length of motor case [m]
σ_1	=	motor case hoop stress [Pa]
σ_2	=	motor case longitudinal stress [Pa]

I. Introduction

This thesis project represents the initial stages of a potentially on-going investigation within UNSW@ADFA into the science and engineering behind solid-propellant rocket motors. Solid-propellant rocket motors are a very effective and relatively simple method of propulsion. They have many useful applications, ranging from amateur model rocketry to boosting payloads into space. They also have many useful military applications, especially within the Australian Defence Force's (ADF) weapons inventory. The ADF have a number of weapons that are propelled by solid-propellant rocket motors. These include the RIM-162 Evolved Sea Sparrow Missile (ESSM) used by the Navy, RBS 70 Man-Portable Air-Defence System (MANPADS) used by the Army, and AIM-9 Sidewinder heat-seeking missile used by the Air Force (*Australian Government Department of Defence website*, viewed 29 Sep 08). This thesis topic provides a means for introducing general knowledge on solid-propellant rocket motors into the ranks of the ADF, which is a beneficial prospect for the ADF. The advantage of conducting small-scale solid-propellant rocket motor research/investigations is that the same theory applies to motors of all scales. Small-scale 'microrocket' motors have been produced with typical thrusts in the order of 0.001 N (Rossi, Orieux, Larangot, Do Conto & Esteve, 2002, p125) whilst the largest, most powerful solid-propellant motor ever produced is the Space Shuttle's Solid Rocket Booster (SRB) with a maximum thrust of 14.7 million N (Heath & Dick, 2000, p24). The fact that the same principles apply to motors of any scale means that solid-propellant rocket motor experiments and research can be conducted using small, scaled-down motors for convenience, safety and cost-saving while the findings can be applied to large, full-scale motor applications (Sutton & Biblarz, 2001, p427). For this reason, it was deemed that it would be useful to explore the specifications of the small black-powder (gunpowder) rocket motors manufactured by the US-based company, *Estes Industries*, as an initial stage of the thesis topic.

In order to set achievable thesis goals given the broad nature of the thesis topic, the project was broken into three specific phases. The first phase, or phase one, aimed to confirm the performance of selected sizes of Estes rocket motors claimed by Estes in their product catalogue (refer to Figure 3). This involved designing and constructing a thrust-measuring instrument to measure the actual thrust-time profiles generated by two selected sizes of rocket motors and to compare these results against the thrust-time profiles and performance figures given in the Estes product catalogue (Figure 3). The second phase of the thesis aimed to determine the temperature sensitivity of motor performance of one size of Estes motor. The results were qualified and quantified using rocket theory and compared with typical temperature sensitivities of other commercially-produced solid-propellant rocket motors. The third or final phase of the thesis aimed to design, construct and test two home-made solid-propellant rocket motors. The intention was to design two motors with the same performance as the Estes motors used in the first two phases of the thesis. A home-made propellant recipe was extracted from Sleeter, 2004, p252. The design of the home-made motors involved applying thermodynamic nozzle theory and by making a number of assumptions about the combustion of the home-made propellant. Finally, the thrust-measuring instrument used in the first and second phases of the thesis project was used to measure the thrust-time profiles of the home-made motors, thus, enabling a comparison with the black-powder Estes motors. Commercially produced model rocket motors, such as Estes products, are very reliable; however, they are expensive to the amateur model rocket enthusiast (refer to Appendix R), especially considering the motor casing is non-reusable. If a reusable home-made solid-propellant rocket motor could be designed, constructed and launched for a much lower cost than that of the commercially-produced motors while still being competitive in the areas of performance, reliability, safety and convenience, then this home-made motor would be a very attractive alternative to purchasing expensive motors from hobby shops.

II. Background Theory

A. Introduction to Solid-Propellant Rocket Motors

In solid-propellant rocket motors, the propellant to be burned is contained within the combustion chamber or motor case. The motor case is effectively a pressure vessel that is designed to contain the high gas pressures required for propellant combustion which for black-powder propellant is in the range of 0.69 MPa to 6.9 MPa (Zaehringer, 1955, p38). The solid propellant charge is called the grain and it contains all the chemical elements for complete burning (i.e. oxidizer, fuel, binder, burn-rate modifier etc.). Sectional diagrams of a typical solid-propellant rocket motor and an Estes motor can be seen in Figures 1 and 2 respectively. Once ignited by the ignition system (which is usually an electrical fuse), the grain usually burns smoothly at a predetermined rate on all exposed surfaces of the grain. The exposed grain surfaces continue to recede in a direction perpendicular to the exposed surfaces until the propellant is totally consumed. The resulting hot gas flows through the convergent-divergent supersonic nozzle to impart thrust. For most solid-propellant motors, once they are ignited they cannot be extinguished and the thrust cannot be randomly throttled in any way. Almost all solid-propellant rocket motors are used only once. The hardware that remains after all the propellant has been burned and the mission completed—namely the nozzle, case, or thrust vector control device—is not reusable (Sutton & Biblarz,

2001, p6). In very rare applications, such as the Shuttle SRBs, is the hardware recovered, cleaned, refurbished, and reloaded. Reusability makes the design more complex, but if the hardware is reused often enough a major cost-saving will result (Sutton & Biblarz, 2001, p419). Case reusability was a desired design requirement of the home-made rocket motor produced in this thesis, albeit on a much smaller scale.

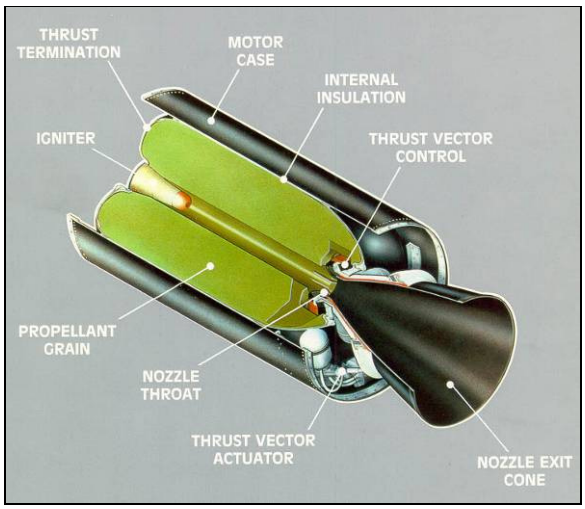

Figure 1. Sectional diagram of a typical solid-propellant rocket motor design (Purdue University, viewed 27 Apr 08). *This figure shows the various common components of most solid-propellant rocket motors.*

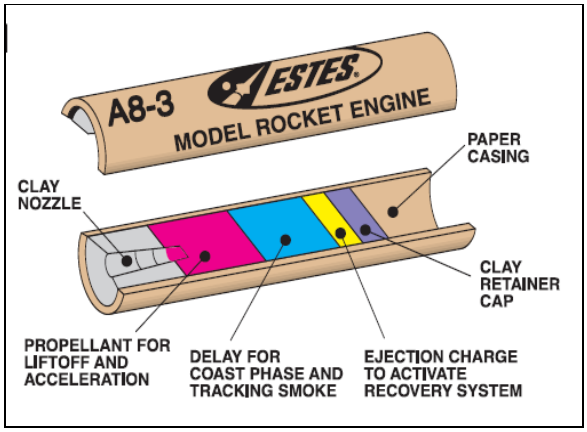

Figure 2. Estes motor design (Estes Catalogue, 2006, p34). *This figure shows the various common components of the Estes range of black-powder rocket motors.*

B. Rocket Propulsion Principles

Rocket propulsion principles are essentially those of mechanics, thermodynamics, and chemistry. Propulsion is achieved by applying a force to a vehicle in the direction of intended travel. For rockets, this propulsive force is obtained by ejecting propellant at high velocity out of a nozzle. Rocket propulsion principles include; propulsive force, exhaust velocity, and the efficiencies of creating and converting system energies.

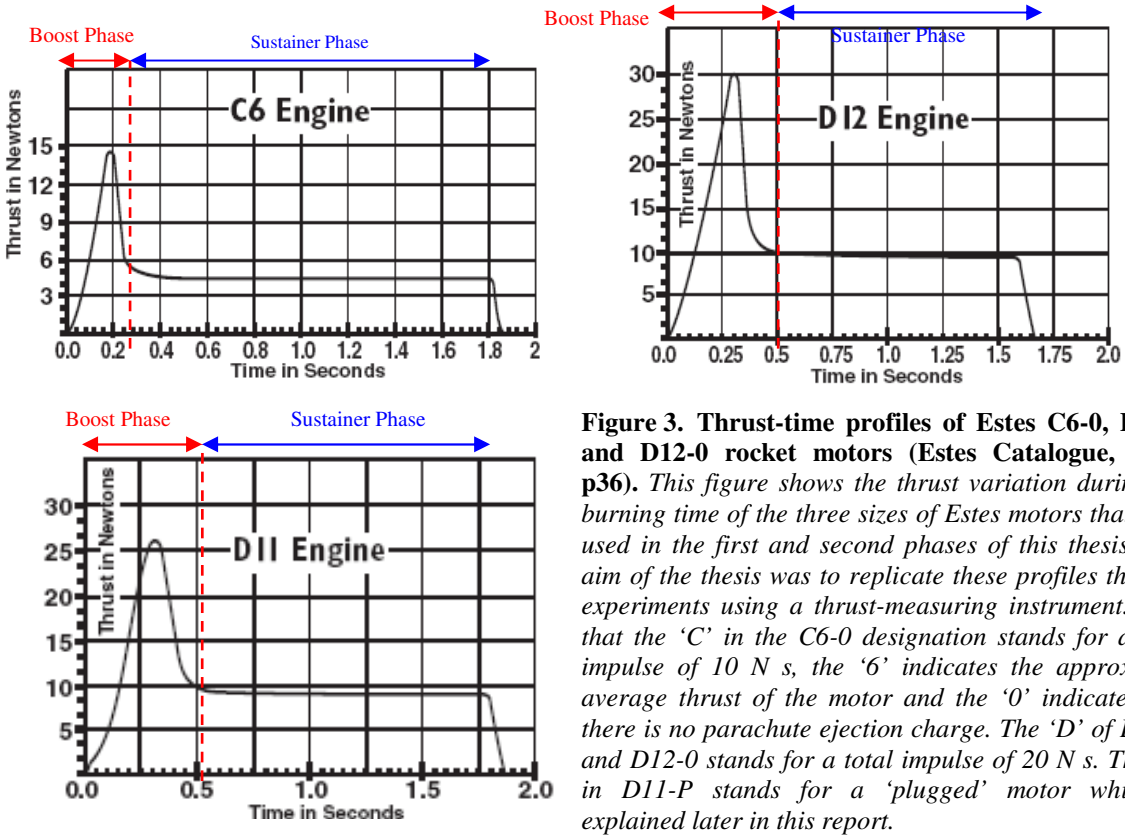

Figure 3. Thrust-time profiles of Estes C6-0, D11-P and D12-0 rocket motors (Estes Catalogue, 2006, p36). *This figure shows the thrust variation during the burning time of the three sizes of Estes motors that were used in the first and second phases of this thesis. One aim of the thesis was to replicate these profiles through experiments using a thrust-measuring instrument. Note that the 'C' in the C6-0 designation stands for a total impulse of 10 N s, the '6' indicates the approximate average thrust of the motor and the '0' indicates that there is no parachute ejection charge. The 'D' of D11-P and D12-0 stands for a total impulse of 20 N s. The 'P' in D11-P stands for a 'plugged' motor which is explained later in this report.*

1. Impulse and Mass Fraction

The total impulse, I_T [N s], is the thrust force, F [N] (which can vary over time as seen in Figure 3), integrated over the burning time of the propellant grain, t_b [s]:

$$I_T = \int F\,dt \quad \text{for} \quad 0 \le t \le t_b \tag{1}$$

I_T is proportional to the total energy released by all the propellant in a solid rocket motor. I_T for the 'C' size and 'D' size Estes rocket motors are 10 N s and 20 N s respectively. The specific impulse, I_s [s], is the total impulse per unit weight of propellant. I_s is an important performance parameter of a rocket motor and a higher value means better performance. Specific impulse is actually a propellant property where high specific impulses are achieved through high gas temperatures and/or low molecular mass of propellant components (Sutton & Biblarz, 2001, p480).

$$I_s = (\int F\,dt) / (\int g_0 \dot{m}\,dt) \tag{2}$$

where $\dot{m}$ [kg s^{-1}] is the propellant mass flow rate and g_0 [m s^{-2}] is acceleration due to gravity. This equation will give a time-averaged specific impulse value for any rocket motor, particularly where the thrust varies with time (Sutton & Biblarz, 2001, pp27-28).

In a rocket nozzle the actual exhaust velocity is non-uniform over the entire exit cross-section and does not represent the entire thrust magnitude. The velocity profile is difficult to measure accurately and was not an aim of this thesis. For convenience, a uniform axial velocity, c is assumed which allows a one-dimensional description of the problem. This effective exhaust velocity, c [m s^{-1}], is the average equivalent velocity relative to the motor case at which propellant is ejected from the nozzle over the total burn time, t_b. It is defined in the following way:

$$c = I_s g_0 \tag{3}$$

Since c and I_s differ only by an arbitrary constant, g_0, either one can be used as a measure of rocket performance. In solid propellant rockets it is difficult to measure the propellant flow rate accurately. Therefore, the specific impulse is often calculated from the total impulse and the propellant weight (found using the difference between initial and final motor weights). In turn the total impulse is obtained from the integral of the measured thrust-time relationship (Sutton & Biblarz, 2001, p29).

The propellant mass fraction, ζ, indicates the fraction of propellant mass, m_p [kg], in a motor initial mass, m_0 [kg] (this fraction can also be applied to an entire vehicle or vehicle stage). When applied to a rocket motor, the value of the propellant mass fraction, ζ, indicates the quality of the motor design, thus, will be a suitable comparison indicator when comparing the Estes motors with my home-made motors. A high value of ζ is desirable as it indicates a structurally efficient design (Sutton & Biblarz, 2001, p30).

$$\zeta = m_p/m_0 \tag{4}$$

m_p for the Estes 'C' size and 'D' size motors is 12.48 g and 24.93 g respectively. m_0 for the C6-0 and D12-0 motors is 22.7 g and 40.9 g respectively. These values were determined from the Estes Catalogue, 2006, p35 and the motor firings detailed below.

2. Thrust

The thrust produced by a rocket motor can be thought of as the reaction experienced by its motor case due to the ejection of matter at high velocity. This 'reaction' phenomenon is more correctly stated as conservation of momentum. Momentum is a vector quantity and is defined as the product of mass times velocity. Rockets generate their forward momentum at the expense of the momentum of the ejected propellant products, which are accelerated towards the rear by the motor convergent-divergent nozzle. Over a small amount of time, the mass of the ejected exhaust gases is relatively small compared with the instantaneous mass of the rocket; however, it is the magnitude of the exhaust gas velocity that imparts such a large change in momentum on the rocket, and therefore, such large accelerations. The thrust, due to change in momentum, is given below (Sutton & Biblarz, 2001, p32):

$$F = \dot{m}v_2 \tag{5}$$

where v_2 [m s^{-1}] is the instantaneous exhaust velocity relative to the motor case. This force represents the total propulsion force when the nozzle exit pressure equals the ambient pressure. The pressure of the surrounding atmosphere gives rise to the second contribution that influences the thrust. Figure 4 shows schematically the external pressure acting uniformly on the outer surface of a rocket chamber/case and the gas pressures on the inside of a typical solid propellant rocket motor. The size of the arrows indicates relative magnitude of the pressures and velocities. A summation of all the pressure-surface vectors will yield an overall pressure thrust. The total thrust, F_T [N], produced by the motor can be given by:

$$F_T = \dot{m}v_2 + (p_2 - p_3)A_2 \quad (6)$$

The first term on the RHS of equation (6) is the momentum thrust represented by the product of the propellant mass flow rate and its exhaust velocity relative to the motor case. The second term represents the pressure thrust consisting of the product of the cross-sectional area at the nozzle exit, A_2 [m^2] (where the exhaust jet leaves the motor), and the difference between the exhaust gas pressure at the exit, p_2 [Pa], and the ambient fluid pressure, p_3 [Pa]. If the exhaust pressure is less than the surrounding fluid pressure, the pressure thrust is negative. Because this condition gives a lower thrust and is undesirable, the rocket nozzle is usually so designed that the exhaust pressure is equal (nozzle with 'optimum expansion ratio') or slightly higher (under-expanded nozzle) than the ambient atmospheric pressure (Sutton & Biblarz, 2001, pp32-33).

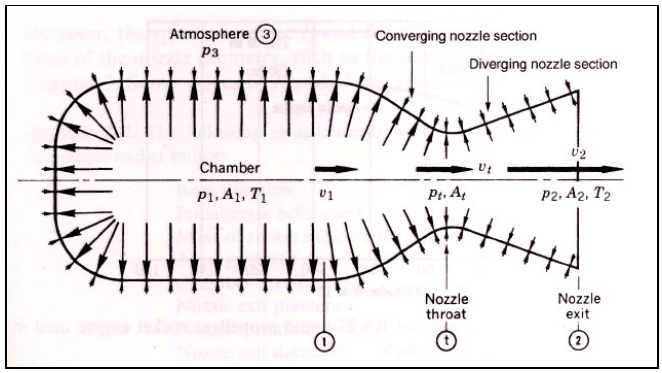

Figure 4. Pressure balance on solid-propellant rocket motor case and nozzle (Sutton & Biblarz, 2001, p33).

The above mentioned theory can quite easily be applied to small solid-propellant rocket motors.

C. Solid Propellant

As seen in Figures 1 and 2, the motor grain is the solid body of the hardened propellant and typically accounts for 82% to 94% of the total motor mass (55% to 60% of the total motor mass for the C6-0, D11-P and D12-0 Estes motors used in this thesis according to Estes Catalogue, 2006, p35). Grains can have many geometry types including slots, grooves, holes, or even no cavities at all which are known as end-burning grains such as the Estes motors (refer to Figure 2). End-burning grains burn solely in the axial direction and maximises the amount of propellant that can be placed in a given cylindrical motor case (Sutton & Biblarz, 2001, p451). Various grain geometry types and associated thrust-time profiles can be seen in Figure 5. The various grain geometries alter the initial burning surface, which determines the initial mass flow rate and the initial thrust. The hot reaction gases of the burnt propellant flow along the perforation or grain cavity toward the nozzle (Sutton & Biblarz, 2001, pp 417-418). For amateur model rockets where maximum achievable altitude is desired, a high boost thrust is desired to apply initial acceleration, but, as propellant is consumed and the vehicle weight is reduced, a decrease in thrust is desirable; this often reduces the drag losses, and usually permits a more effective flight path (i.e. a greater height reached by the Estes rockets). Therefore, there is a benefit to vehicle mass, flight performance, and cost in having a higher initial thrust during the boost phase of the flight, followed by a lower thrust (often 10% to 30% of the boost thrust) during the sustaining phase of the powered flight (Sutton & Biblarz, 2001, p451). This principle has been applied to the Estes motors as seen in Figure 3. It is also possible that a larger concentration of burn rate catalyst (sulfur) was mixed into the initial boost stage of the Estes motor propellant (black-powder) which would also generate a high initial boost thrust.

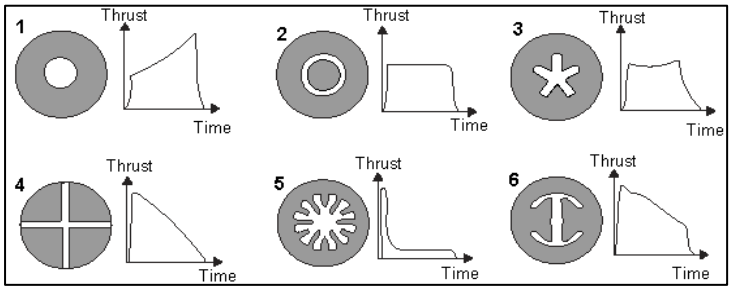

Figure 5. Various typical propellant grain cross-sections and associated thrust-time profiles (ALLSTAR Network, viewed 27 April 08). *The shape of the thrust-time profile depends on how the grain exposed surface area changes over the motor's burn time.*

The Estes rocket motor propellant is tightly compacted black-powder, more commonly known as 'gunpowder'. Most black-powders contain 75% of potassium nitrate (KNO_3) or sodium nitrate ($NaNO_3$) which acts as the oxidiser, 15% of charcoal or some form of carbon (C) as the fuel, and 10% sulphur (S) which acts as both a fuel and burn rate catalyst (Zaehringer, 1955, p38). Black-powder has an auto-ignition temperature of about 464°C (MSDS-BP, 2005, p1) and becomes hygroscopic (absorbs water) at humidities exceeding 90% and then rapidly ceases to burn (Fordham, 1980, p165). For this reason, Estes rocket motors should be disposed of in water as this saturates the black-powder and renders the motor useless (Estes Model Rocket Engine and Igniter Instructions, 2001-2003). In general, if the carbon content is too low a readily ignited black-powder is obtained but it has slow burning properties. If the carbon content is too high, the black-powder will be difficult to ignite and irregular in burning. The burning rate of the powder can also be varied by changing the potassium nitrate content. The maximum burning rate is usually obtained at a potassium nitrate content of rather less than 70%. The burning rate, r [m s^{-1}], of black-powder depends exponentially on the chamber pressure, p_1 [Pa], by the following equation, known as Vieille's law or Saint Robert's law:

$$r = ap_1^{\,n} \tag{7}$$

where both a and n are empirically-determined constants (Fordham, 1980, p166). The constant, a, is affected by the initial grain temperature and the constant n determines how sensitive the burn rate is to chamber pressure. The burn rate of the black-powder in the Estes motors used in this thesis project was calculated to be approx. 0.030 m s^{-1} (refer to Appendix O). Factors affecting burn rate include; propellant type, oxidizer to fuel ratio, oxidizer particle size and compaction, ratio of oxidizer particle sizes, burning rate catalysts such as sulphur or imbedded metal wires or staples (Sutton & Biblarz, 2001, p426), heat of combustion of the binder, chamber pressure, propellant initial temperature, flame temperature, gas velocity through the grain cavity, and motor accelerations (Rochford, 1999, p7). Solid-propellant rocket motors experiencing an acceleration, whether axial or radial, will exhibit an increase in burning rate (Fuchs, Peretz & Timnat, 1982, p539).

Mass flow rate is related to the propellant burn rate by the following equation:

$$\dot{m} = A_b r \rho_b \tag{8}$$

where r is propellant burn rate, A_b [m^2] is the burning area of the propellant grain, and ρ_b [kg m^{-3}] is the solid-propellant density prior to ignition (Sutton & Biblarz, 2001, p427).

D. Temperature Sensitivity of Solid-Propellant Grains

Temperature affects chemical reaction rates and the initial ambient temperature of a propellant grain prior to combustion influences burning rate, as shown in Figure 6. Common practice in developing and testing larger rocket motors is to conduct a temperature sensitivity analysis to ensure that the motor performance characteristics will stay within specified acceptable limits (Sutton & Biblarz, 2001, pp430-431). There are two primary temperature sensitivity coefficients of interest; the temperature sensitivity of burning rate at constant pressure, σ_p [K^{-1}], and the temperature sensitivity of pressure at constant motor geometry, π_K [% $°C^{-1}$]. The temperature sensitivity of burning rate is defined as the change in burning rate for a given change in propellant initial temperature at constant chamber pressure, p. The temperature sensitivity of pressure is defined as the change in combustion-chamber pressure for a given change in propellant initial temperature at constant propellant burning area to nozzle throat area ratio, K. For a particular propellant and motor type, the relationship between combustion-chamber pressure, p (which is directly related to the thrust), and motor burning time, t_b, varies with initial grain temperature as indicated in Figure 6 (Rochford, 1999, pp7-8).

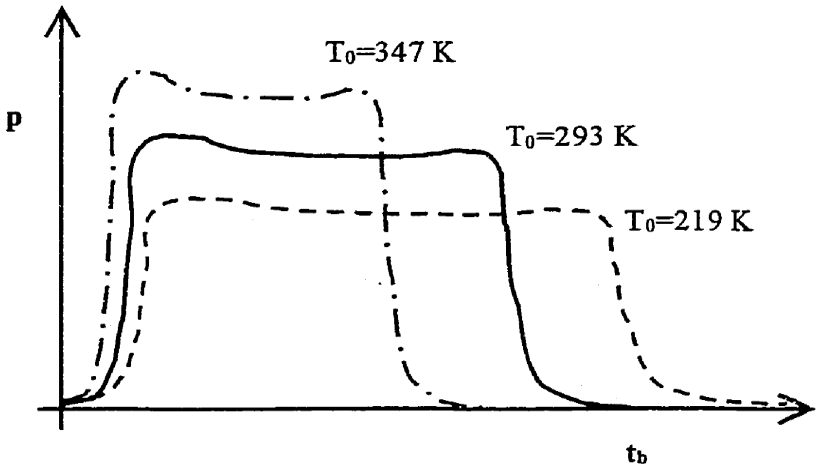

Figure 6. Temperature sensitivity of burning rate at various initial propellant temperatures (Rochford, 1999, p8). *The figure shows that the propellant burn time, t_b, decreases (or burn rate, r, increases) with increasing initial propellant temperature, T_0. The average chamber pressure increases with increasing initial propellant temperature.*

The definition of σ_p is as follows:

$$\sigma_p = (\partial \ln r/\partial T_0)_p \quad \text{or} \quad \sigma_p \approx ((\ln r_2 - \ln r_1)/(T_{02} - T_{01}))_p \tag{9}$$

where r is the propellant burn rate, T_0 [K] is the propellant initial temperature, and subscripts 1 and 2 indicate measurements taken at two different initial temperatures. The subscript p indicates at constant chamber pressure (Rochford, 1999, p9). Typical values of σ_p are 0.001 to 0.009 per degree Kelvin [K^{-1}] (Sutton & Biblarz, 2001, p432). For a given pressure-time variation such as in Figure 6, dynamic burning is enhanced by larger values of σ_p; propellants with high σ_p, tend to extinguish easily, ignite with greater difficulty and are prone to combustion instabilities (Kuo & Coates, 1977, p1187). The definition of π_K is as follows, where typical values of π_K are 0.067 to 0.278 percent per degree Celcius [% $°C^{-1}$] (Sutton & Biblarz, 2001, p432):

$$\pi_K = (\partial \ln p/\partial T_0)_K \quad \text{or} \quad \pi_K \approx ((\ln p_2 - \ln p_1)/(T_{02} - T_{01}))_K \tag{10}$$

where the subscript K indicates at constant ratio of burning surface area, A_b, to nozzle throat area, A_t [m^2], by the following relation (Rochford, 1999, p9):

$$K = A_b/A_t \tag{11}$$

As end-burning grains have a relatively constant burning surface area over the motor's burn time, π_K was used instead of σ_p for analysing the results of the temperature sensitivity of the end-burning Estes motor performance during phase two of the thesis. As equations 5 and 8 show that burn rate is directly related to thrust and Appendix N shows that chamber pressure is directly related to thrust, it follows that the temperature sensitivity of burn rate is directly related to the temperature sensitivity of chamber pressure. The relationship between σ_p and π_K is given by the following relation:

$$\pi_K = \sigma_p/(1-n) \tag{12}$$

where n is the constant pressure exponent as found in equation 7 (Rochford, 1999, p9).

E. Rocket Performance Testing

Before solid-propellant rocket motors are put into operational use, they are subjected to several different types of tests. These tests can include; manufacturing inspection and fabrication, component tests, static rocket system tests, static vehicle tests, and flight tests, and are generally conducted in that order (Sutton & Biblarz, 2001, p711). In terms of performance testing of a rocket motor, it is obvious that flight tests would give the most meaningful performance results; rocket motors are designed and built to experience accelerations during flight in constantly changing environmental conditions (temperature, pressure, humidity, atmospheric gas composition

etc.). Sometimes it is not feasible to conduct a flight test and static tests must be implemented instead. A static test is defined as testing or operating a motor in a fixed, non-mobile position. Thus, the motor is usually fastened to a test stand and not allowed to move during the test. The forces, pressures, temperatures, etc., are then measured and recorded during firing. Of all the fundamental quantities of a rocket motor, thrust is rather easily and accurately produced and controlled for calibration purposes. During a thrust-measuring test the motor is held fast to the test stand, although the stand itself is free to move to allow transfer of thrust from the motor to the measuring or thrust-sensitive element (Zaehringer, 1955, p93).

Force or thrust-sensitive elements or transducers are of three types; electrical, hydraulic, and mechanical. The electrical type is the most versatile and widely used for rocket motor tests. In the electrical force transducer, force or thrust on a load-sensitive element causes some change in its electrical properties (i.e. resistance, capacitance etc.). Because of their excellent reliability, the strain-gauge type of transducer (e.g. load cells) has become very popular in rocket testing. In a hydraulic system, the thrust acts through a piston of known area and produces a known pressure which is displayed or recorded. Since pressure is force per unit area, the thrust can be determined. This type of system is characterised by simplicity, ruggedness, and low cost. However, the frequency response is poor and operating pressure and thrust-alignment are critical factors. Mechanical force systems employ the use of springs, scales, etc. For any system where the thrust changes rapidly, the use of springs and scales is questionable as the frequency response of mechanical systems is poor. A spring-type mechanical system, however, is simple and can be used to advantage for measurements not requiring high accuracy. The calibration of thrust transducers is merely a matter of applying a known force or weight to the system and noting a change in electrical, hydraulic, or mechanical response (Zaehringer, 1955, p95).

F. Instrumentation and Measurement

A thrust-measuring system usually requires one or more sensing elements (transducers), a device for recording, displaying and/or indicating the thrust-time relationship, and often another device for conditioning, amplifying, correcting, or transforming the transducer signal into a form suitable for recording, indicating, display, or analysis. Recording of rocket test data has been performed in several ways, such as on magnetic tapes or disks or by computers (Sutton & Biblarz, 2001, p720). *Range* of a thrust measuring system refers to the region extending from the minimum to the maximum thrust the system can measure. The range is usually limited by instrument yield strength and/or the *linear operating range*. The linear operating range implies that the system will become increasingly nonlinear beyond the maximum and minimum limits. Usually an additional margin is provided to permit temporary overloads without damage to the system or need for recalibration and to ensure measurements lie in the system linear range (Tse & Morse, 1989, p54). *Resolution* refers to the minimum change in the measured thrust that can be detected with a given instrument.

Errors in measurements are usually of two types: (i) *human errors* of improperly reading the instrument, chart, or record and of improperly interpreting or correcting these data, and (ii) *instrument or system errors*, which usually fall into four classifications: static errors, drift errors, dynamic response errors, and hysteresis errors. *Static errors* are usually fixed errors due to fabrication and installation variations; these errors can usually be detected by careful calibration, and an appropriate correction can then be applied to the reading (Sutton & Biblarz, 2001, p271). *Drift error* is the change in output over a period of time, usually caused by random wander and environmental conditions. All instruments will drift to a certain degree. The long-time drift of an instrument is a part of its specifications (Tse & Morse, 1989, p47). To avoid drift error the instrument has to be calibrated at frequent intervals at standard environmental conditions against known standard reference values of its whole range (Sutton & Biblarz, 2001, p271).

Dynamic response errors occur when the measuring system fails to register the true value of the measured quantity while this quantity is changing, particularly when it is changing rapidly. For example, the thrust force has a dynamic component due to vibrations, combustion oscillations, interactions with the support structure, etc. These dynamic changes can distort or amplify the thrust reading unless the test stand structure, the rocket mounting structure, and the thrust measuring and recording system are properly designed to avoid harmonic excitation or excessive energy damping. To obtain a good dynamic response requires a careful analysis and design of the total system (Sutton & Biblarz, 2001, pp721-722). A *maximum frequency response* refers to the maximum frequency, usually in cycles per second or Hertz [Hz], at which the instrument system will measure true values. The natural frequency of the measuring system is usually above the maximum response frequency. Generally, a high-frequency response requires more complex and expensive instrumentation. All of the instrument system (sensing elements, modulators and recorders) must be capable of a fast response. Most of the measurements in rocket testing are made with one of two types of instruments: those made under nearly steady static conditions, where only relatively gradual changes in the quantities occur, and those made with fast transient conditions, such as rocket starting, stopping, or vibrations. This latter type of instrument has frequency responses above 200 Hz, sometimes as high as 20,000 Hz. These fast measurements are necessary to evaluate

the physical phenomena of rapid transients. *Linearity* of the instrument refers to the ratio of the input (usually pressure, temperature, force, etc.) to the output (usually voltage, output display change, etc.) over the range of the instrument. Very often the static calibration error indicates a deviation from a truly linear response. A nonlinear response can cause appreciable errors in dynamic measurements (Sutton & Biblarz, 2001, pp721-722). Dynamic errors cannot be subtracted from the measured data because a quantitative dynamic error for measurements cannot be deduced. This is because knowing how much each type of system error contributes to the overall measurement error is impossible. The dynamic error can only be observed by applying a known dynamic test signal to the instrument and noting the deviations at the output or by comparing the output of a test instrument with that of a reference in much the same way as the thesis has compared the measured thrust-time plots against the thrust-time plots provided by Estes (refer to Figure 3). The observations may show the deviations but do not give a numerical value for the transient error (Tse & Morse, 1989, pp198-199).

Dead zone or *hysteresis errors* are often caused by energy absorption within the instrument system or play in the instrument mechanism; in part, they limit the resolution of the instrument. *Sensitivity* refers to the change in response or reading caused by special influences. For example, the temperature sensitivity and the acceleration sensitivity refer to the change in measured value caused by temperature and acceleration. These are usually expressed in percent change of measured value per unit of temperature or acceleration. This information can serve to correct readings to reference or standard conditions (Sutton & Biblarz, 2001, p722). Electrical interference or *noise* within an instrumentation system, including the power supply, transmission lines, amplifiers, and recorders, can affect the accuracy of the recorded data, especially when low-output transducers are in use (Sutton & Biblarz, 2001, p722). Electrical noise occurs as a result of magnetic fields generated by current flow in wires in close proximity to the small wires inside a transducer or the lead wires, which are wires used to connect a transducer to the instrumentation system (Dally, Riley & McConnell, 1993, p18). In some instances, the voltage induced by the magnetic field is so large that the signal-to-noise ratio becomes problematic and it is difficult to separate the noise from the transducer signal. There are three ways of maximising the signal-to-noise ratio. These are; (i) all lead wires should be twisted, (ii) only shielded cables should be used and the shields should be grounded, and (iii) differential amplifiers should be used to reduce noise by destructive interference of the noise signal (Dally, Riley & McConnell, 1993, pp234, 236).

III. Phase One — Confirming the Thrust-Time Profiles of the Estes Motors

This first phase of the thesis project aimed to confirm the performance of C6-0 and D12-0 Estes rocket motors claimed by Estes in their product catalogue. This involved designing and constructing a thrust-measuring instrument to measure the actual thrust-time profiles generated by C6-0 and D12-0 sizes of rocket motors and to compare these results against the thrust-time profiles and performance figures published in the Estes product catalogue.

A. The Thrust-Measuring Instrument

1. Design of the Thrust-Measuring Instrument

During the initial stages of this thesis project, it was identified that the primary design requirements for the thrust-measuring instrument should be simplicity and accuracy. The life of the thesis project was relatively short, hence the need for a simple, easy-to-construct, easy-to-use instrument. It was also identified that the thrust produced by the Estes rocket motors was relatively small compared with typical, everyday forces, hence the need for an accurate and sensitive instrument that would achieve the required resolution in thrust measurements. Initial discussions with my thesis supervisors, Dr. John Milthorpe and Dr. Neil Mudford, yielded four physics principles/methods that could be applied to the instrument design to determine motor thrust. These methods were; (1) measuring strain in a deflecting material, (2) measuring angular displacement or angular velocity, (3) measuring the transmission of pressure, and (4) measuring axial acceleration of an unrestrained rocket motor. Further to these discussions, a literature review of previous and existing rocket thrust-measuring instruments was conducted to begin formulating some ideas on the potential solution. Details of this literature review can be found in Appendix G.

After much consideration and analysis with calculations (refer to Appendices A to G), I decided that a modified version of method (1) mentioned above was the best option. Instead of applying strain-gauges directly to a deflecting cantilever beam where the amount of beam deflection is dependent on the motor thrust, it was identified that measuring the strain in a separate load-cell type transducer under a hinged-cantilever beam would eliminate many of the undesirable transient affects created during the motor firings. It was discovered that suitable XTRAN load-cells (manufactured by *Applied Measurement Australia*) were available for this thesis project from SACME. The advantage of having a hinged-cantilever beam resting on a load-cell rather than having strain-gauges directly applied to a rigid, deflecting cantilever beam is that the load-cells are designed to

deflect a minimal amount, such that beam excitation, beam inertia and delayed response would not be a major problem. Given that the load-cell available to the thesis was rated at 250 N maximum allowable load and that the average thrust of the C6-0 motor was 6 N, it was identified that the load-cell may not have enough *resolution* to capture the exact detail of the Estes thrust-time profiles. According to the XTRAN 'S'-type load-cell data sheet, the load-cell has a resolution of 0.1% of the load applied. This should be sufficient; however, to be certain that the required resolution was achieved; the instrument design utilized a hinged, rigid, steel cantilever beam to mechanically amplify the thrust of the rocket motor at the load-cell position along the beam by creating a moment arm. The cantilever beam was designed to be very stiff and rigid in the transverse direction (high second moment of area) to prevent significant deflection in the instrument (refer to Appendix F), but also to ensure that the natural frequency of the beam was much larger than the frequency of the motor's boost phase to prevent resonance (refer to Appendices A and B). The mass of the beam was monitored during its design to ensure that the weight of the beam resting on the load-cell plus the maximum thrust of the larger D12-0 motor did not exceed the maximum load of the load-cell. As can be seen in Appendix F, a factor of safety of 1.5 was factored into the calculations to ensure that the load-cell was not overstressed even if the thrust spiked at a larger-than-expected value during the tests. Another advantage of the hinged-cantilever beam design was that it separated the motor and load-cell by a sufficient distance such that the heat produced in the material immediately surrounding the motor during firing would not damage the internal electronic workings of the load-cell. It was deemed that the friction in the hinge of the beam would be negligible relative to the forces produced by the rocket motors. Because there were no major disadvantages identified for this design and that the design was easy to construct and operate, it was selected as the best thrust-measuring instrument design after many discussions with the thesis supervisors.

2. Mock-Up Instrument Trial

A rough mock-up of the instrument was constructed and tested to ensure that there were no unexpected design flaws before the final, refined instrument was produced. Two actual motor firings were conducted using the mock-up instrument which produced good results that closely match the results I was expecting for the Estes D11-P motors. The D11-P motors were used instead of the C6-0 or D12-0 motors as it was found that if unrestrained, the C6-0 and D12-0 motors would eject out of the motor-holder cup at high velocity towards the end of the motor burn time. This was due to the combustion-chamber pressure exceeding the strength of the propellant end-seal once the propellant was almost totally consumed (refer to Appendix H). The D11-P is a 'plugged' motor (hence the 'P' designation) and the plug was able to withstand the combustion-chamber pressures, enabling the D11-P motors to remain in the motor-holder cup even when unrestrained. A photo of the mock-up instrument can be seen in Figure 7 and some of the results obtained using the mock-up instrument can be seen in Figure 8. The rest of the mock-up instrument-trial results can be found in Appendix K. As can be seen from Figure 8, the results are smooth, are not masked by large amounts of noise, are consistent and are very similar to the thrust-time profile claimed by Estes for the D11-P motors (refer to Figure 3). In an attempt to reinforce the propellant end-seal of the C6-0 and D12-0 motors to prevent the chamber pressure from splitting the end-seal open, water-based putty was packed into the top of the motor case against the seal and left to dry. This, in conjunction with a motor-restraining method that was implemented on the refined-version of the thrust-measuring instrument, prevented the C6-0 and D12-0 motors from ejecting out of the motor-holder cup in future tests.

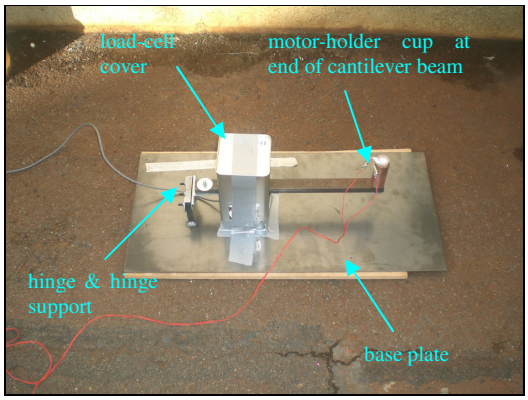

Figure 7. Rough mock-up thrust-measuring instrument. *This instrument was constructed out of readily available materials using quick yet imprecise manufacturing techniques such as welding the hinge support to the base plate.*

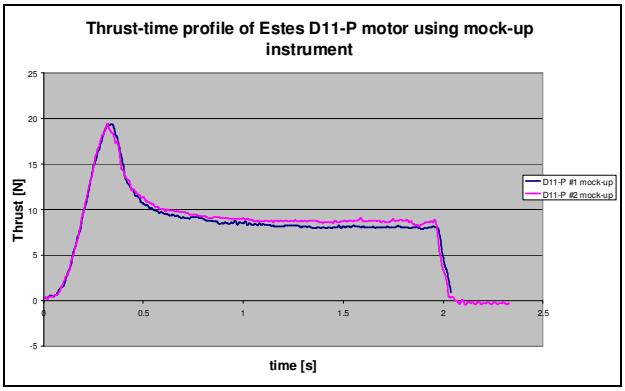

Figure 8. Results from two Estes D11-P motors using the rough mock-up instrument. *Thrust-time profiles were obtained using the mock-up instrument to ensure that the design would give reliable results before a refined version was manufactured. The D11-P motors were used because a motor-restraint method had not been implemented at that stage.*

3. Refined Instrument

As the mock-up thrust-measuring instrument was a successful trial of the chosen instrument design, engineering drawings were developed for a refined, more precise version of the instrument using the CAD program *PTC ProDESKTOP*. These drawings can be found in Appendix I. These drawings were submitted to the SACME main workshop for production. Once the workshop finished construction of the instrument components, I fastened the components together, including fastening the XTRAN 250 N 'S'-type load-cell to the instrument base plate (Figure 10). The refined instrument assembly can be seen in Figure 9.

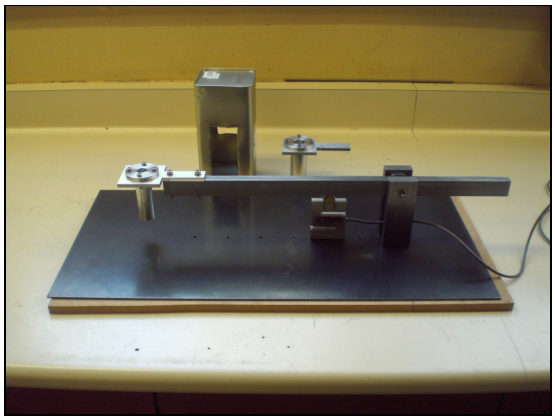

Figure 9. Refined version of the thrust-measuring instrument. *This instrument was constructed by the SACME main workshop to specified dimensions and tolerances. There is much less free-play in this instrument than the mock-up instrument.*

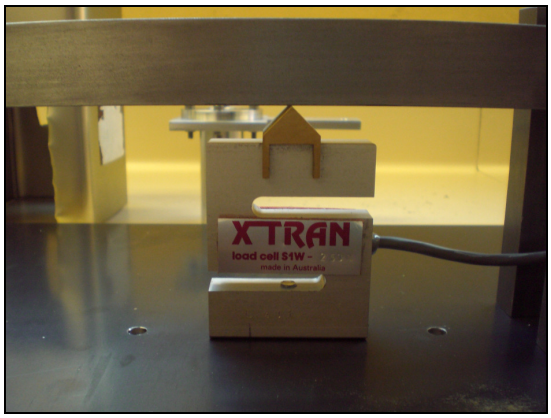

Figure 10. XTRAN 250 N 'S'-type load-cell. *This load-cell transducer has a 10 V (±5 V) input and the electrical output signal is determined by the strain 'felt' in the cell. The cell is designed to deflect a minimal amount.*

4. Experiment Setup

To obtain useful data from the load-cell transducer, a data acquisition (DAQ) system was required as well as an electrical power supply and electronic amplifier/signal conditioner. The DAQ system used for the thesis experiments was developed by *National Instruments*. This DAQ system consisted of a software suite which I installed onto my laptop computer, a channel-conditioning bus board and the necessary electrical cables. The electrical power supply and electronic amplifier/signal conditioner were contained in the one unit (Figure 13). These were analogue and required a digital multimeter to confirm that the input and output signals were of the desired amplitude. Figure 11 displays the experiment setup.

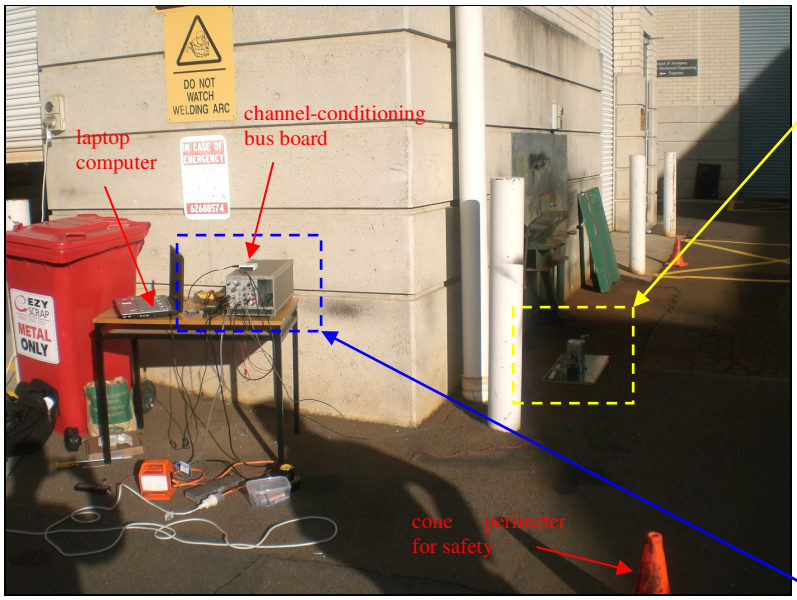

Figure 11. Experiment Setup. *This shows the different components necessary to collect data from the load-cell transducer. For safety, the experiments were usually conducted in the courtyard outside the SACME welding bay and a 5 m radius perimeter of cones was established. Note that the experiment operator was able to stand around the corner of the building from the instrument (at the laptop) in order to block the line-of-sight to the rocket motor firing in case of an explosion and resulting shrapnel.*

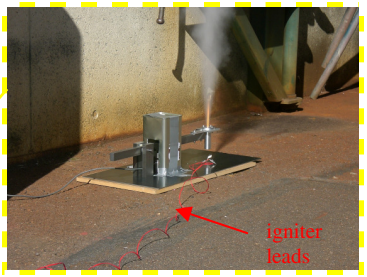

Figure 12. Thrust-measuring instrument.

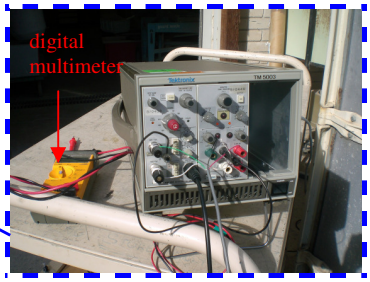

Figure 13. Electrical power supply and electronic amplifier/signal conditioner.

After connecting all of the experiment components, the electronic power supply and amplifier was turned on and left to warm up for approx. 20 minutes. Warming up the power supply/amplifier was required because its output was prone to wander from the set load-cell excitation voltage (±5 V) as its internal circuits went from cold to warm. If the instrument was calibrated immediately after switching the power supply on, then the wander would result in a *drift error* in the thrust results. Once warm and using the digital multimeter, the load-cell excitation voltage was set to ±5 V using the fine output adjustment knobs on the power supply control panel. Before firing the first rocket motor in the instrument for the day, it was necessary to statically calibrate the instrument using exact weights (±0.1 g) making sure to cover the range of expected thrust results. The instrument was calibrated in grams as the thrust data would be converted to Newtons at a later stage. This made the calibration process more efficient and more accurate as it omitted the need to multiply all masses by g_0, which is not exactly 9.81 m s^{-2}. The calibration data was saved using the DAQ software on the laptop. An example of the static calibration of the instrument can be seen in Figure 14. The calibration data obtained over the thesis duration can be found in Appendix J. During the calibration process, it was not critical to know the exact moment-arm lengths of the hinged-cantilever beam resting on the load-cell. To avoid overstressing the load-cell during the calibration process, it was known that the moment-arm to the motor-holder cup was approximately four times the moment-arm to the load-cell position. Given that the

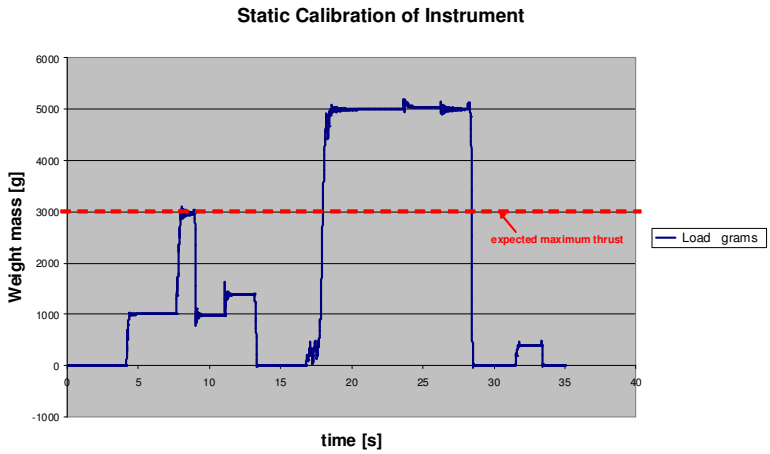

Figure 14. Calibration check of the instrument. *This actual plot was just a check to ensure that the calibration process had worked. The DAQ software displays a linear plot of load vs. output voltage from the load-cell during the calibration process. The linear correlation or linearity, R, is also displayed to the user. I achieved R values of around 0.999990 for all my instrument calibrations (refer to Appendix J).*

maximum allowable load of the load-cell was 250 N, this meant that absolutely no more than 62.5 N (approx. 6250 g) could be applied at the motor-holder cup (tip of the beam). This maximum allowable load was twice as large as the expected maximum thrust of the D12-0 motors.

Once calibrated, the rocket motor could be inserted into the holder cup on the instrument with the nozzle facing up and the restraint applied. The igniter fuse was then inserted into the motor's nozzle and held in place with a plastic plug (Figure 15). The igniter leads were then connected to the igniter and trailed out back to the

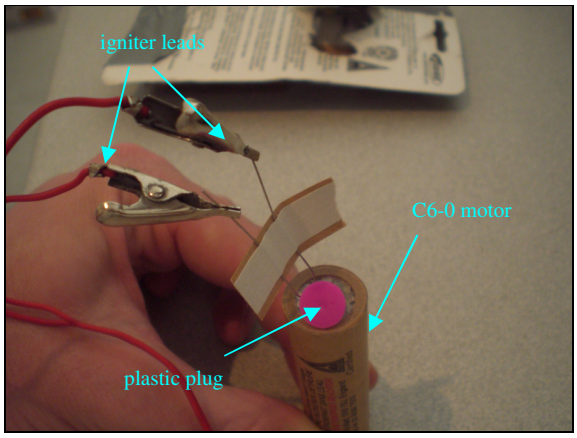

Figure 15. Igniter fuse inserted in motor nozzle.

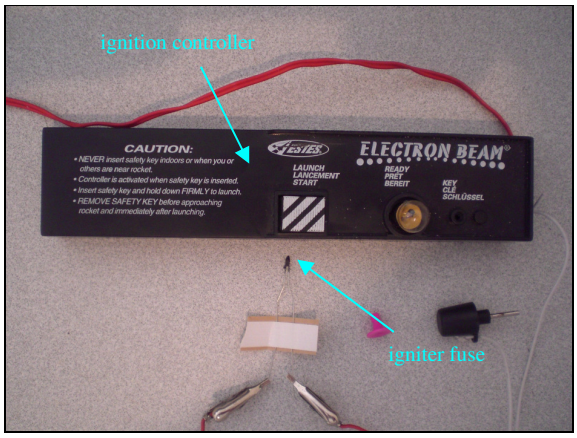

Figure 16. Ignition System.

experiment operator's station at the laptop computer. The 'save' button on the user interface of the DAQ software was clicked and the motor was ignited using the ignition controller (Figure 16) from a safe distance. It is important to note that the data began saving for around 3 seconds before the motor was fired. This was to ensure that the data for the ignition transient phase were not missed. As the motor fired, the thrust pushed down on the hinged-cantilever beam which mechanically amplified the thrust causing a certain amount of strain in the load-cell. The load-cell input excitation voltage from the electrical power supply would be transformed by the change in electrical resistance of the strain-gauges inside the load-cell due to the strain imposed on the load-cell. The load-cell would output the transformed voltage signal which would be received by the electronic amplifier/signal conditioner. The analogue voltage signal would be amplified and conditioned, passed through the channel-conditioning bus board which converts the analogue signal into a digital signal. The digital signal would be passed to the laptop computer via a USB connection and was collected by the DAQ software. The DAQ software collected data over the motor's burn time at a rate of 1000 Hz. The DAQ software averaged every 10 data values to smooth out the data, providing a time interval of 0.01 s, and it automatically stored the data in a *Microsoft Excel* spreadsheet on the laptop.

5. Obtaining the Thrust-Time Profiles

The scaled thrust data stored by the DAQ software required some manipulation to convert into meaningful thrust-time profiles of the motors that were fired. It was identified that when the instrument was calibrated, the mass of the motor case and propellant was not taken into consideration. These masses had to be subtracted from the measured thrust values to give meaningful results. All the motors that were fired were weighed before, m_0 [g], and after, m_f [g], firing. It was also identified that the mass of the propellant remaining in the motor would change over the burn time. In order to simplify the data manipulation, it was assumed that the propellant would be ejected from the motor at a constant rate. The total amount of propellant ejected from the motor over the burn time, m_p [g], was simply given by:

$$m_p = m_0 - m_f \tag{13}$$

Again, this was another assumption made as it is possible that not all of the propellant was burned or that the motor case and nozzle were eroded by the high-velocity, high-temperature combustion gases. The motor burn time start was pinpointed to be where the thrust data first increased continuously above the calibrated zero-thrust value. The motor burnout was pinpointed to be where the thrust data first settled back down at the calibrated zero-thrust value minus m_p. An approximation of the propellant mass flow rate can be given by:

$$\dot{m} = m_p/t_b \tag{14}$$

where t_b is the motor burn time. The thrust data was finally divided by 1000 to convert g to kg then multiplied by the acceleration due to gravity, g_0=9.81 m s^{-2}, to give the thrust data in N. The equation used to manipulate the scaled thrust data, f(t) [g], at a given time, t [s], into a meaningful, adjusted form, $F_T(t)$ [N], was:

$$F_T(t) = (g_0/1000)(f(t) - (m_0 - \dot{m}t)) \quad (15)$$

After applying equation 15 to the scaled thrust-time data, it was found that the thrust values still did not start at zero N or finish at zero N but were out by a common amount depending on which day I conducted the motor test. I took this to be a *static error* in the instrument calibration that varied slightly each time I conducted the calibration. It may have been due to the fact that the linear correlation or *linearity*, R, between the calibration loads applied and the output voltage of the load-cell was not exactly 1.000000 but was more like 0.999990 (the value of R was displayed by the DAQ software after each calibration). To accommodate this static error, I determined an adjustment constant, C [N], for each day I conducted motor firings. By subtracting C from the $F_T(t)$ data obtained during a particular day, I was able to 'zero' the thrust before and after the motor burn time. Not only did this zero the thrust-time profile, but it also enabled a better representation of the actual thrust levels achieved by each motor for a more realistic comparison with the published Estes values. An example of a complete thrust-time profile of a C6-0 motor which was fired in the refined thrust-measuring instrument can be seen in Figure 17.

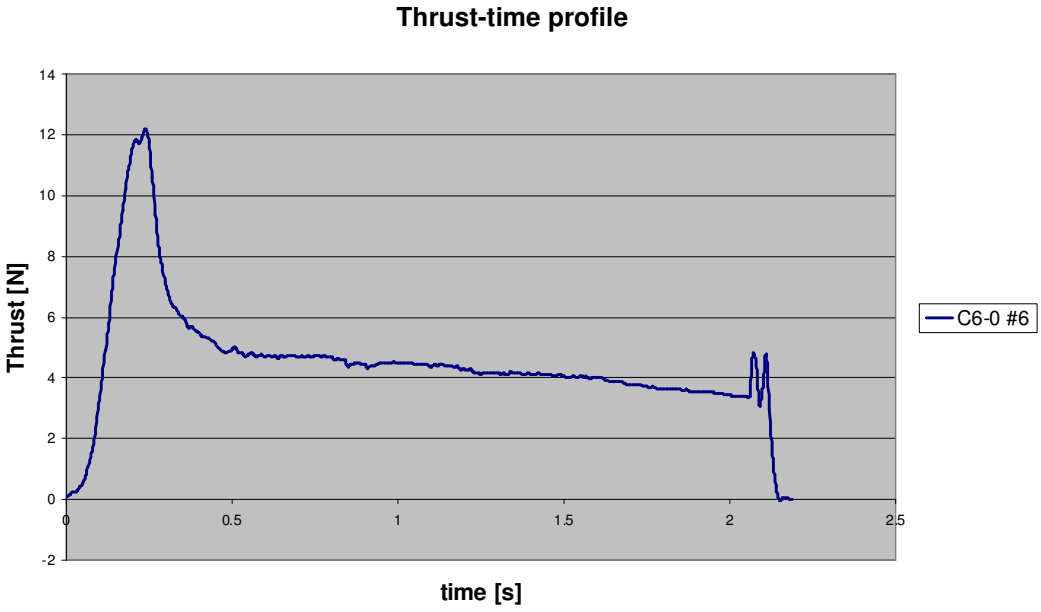

Figure 17. C6-0 thrust-time profile. *This is the thrust-time profile of the sixth C6-0 motor fired in the refined version of the thrust-measuring instrument. The refined-instrument thrust-time profiles were used for the comparison with the published Estes values.*

B. Comparison of Measured Motor Performance with Estes-Claimed Motor Performance

1. Collection and Presentation of the Measured Results

For phase one of the thesis project, I deemed that measuring the results of six C6-0 motors and nine D12-0 motors would enable me to successfully compare my measured results against the results claimed by Estes in their catalogue. Ideally, to obtain the best representation of the distribution and spread of the performance of a particular size of rocket motor, a very large population of motors would need to be tested. Considering that only AU$500.00 of funding from SACME was allocated to this project, this was not a valid option (refer to Appendix R). It was identified that a minimum of three motors of each size would need to be tested to obtain a spread of results that could be analysed and compared with the performance values claimed by Estes. However, only testing three motors was unlikely to provide a reliable spread of results to compare against the Estes values. After weighing up factors including; the cost of the motors, the availability of the motors from the hobby shop, the time constraints of the project, and the amount of motors needed for a reliable comparison with the Estes catalogue, I decided that testing six C6-0 and nine D12-0 motors would provide good results for this phase of the thesis project. The reason I selected to have a different sample population for each size of motor was to

determine whether the larger population would give a significantly better spread of results, therefore, testing whether the extra cost of the larger population would be worth the greater reliability of results.

Once all of the thrust-time profiles for the six C6-0 and nine D12-0 motors were completed, the profiles for each motor size were plotted on the same graph for comparison. From this, it was identified that the ignition transient phase of each motor was different causing the thrust-time profiles not to line-up. Motor ignition is usually completed in a fraction of a second for small rocket motors. The motor chamber pressure rises to an equilibrium state in a very short time, as shown in Figure 18. Conventionally, the ignition process is divided into three phases for analytical purposes. Phase 1, or *ignition time lag*, is the period from the moment the igniter receives a signal until the first bit of grain surface burns. Phase 2, or *flame-spreading interval*, is the time from first ignition of the grain surface until the complete grain burning area has been ignited. Phase 3, or *chamber-filling interval*, is the time for completing the chamber-filling process and for reaching equilibrium chamber pressure and flow (Sutton & Biblarz, 2001, pp524-525). The speeds at which the three phases of the ignition process are completed is dependent on variables such as; igniter fuse characteristics, grain surface roughness, age of the propellant, heat transfer characteristics (or heat flux) by radiation and convection between the igniter gas and grain surface (see Figure 19) and more (Sutton & Biblarz, 2001, pp525-526). A method was required to bring the thrust-time profiles into alignment in order to properly compare the performance spread of the motors.

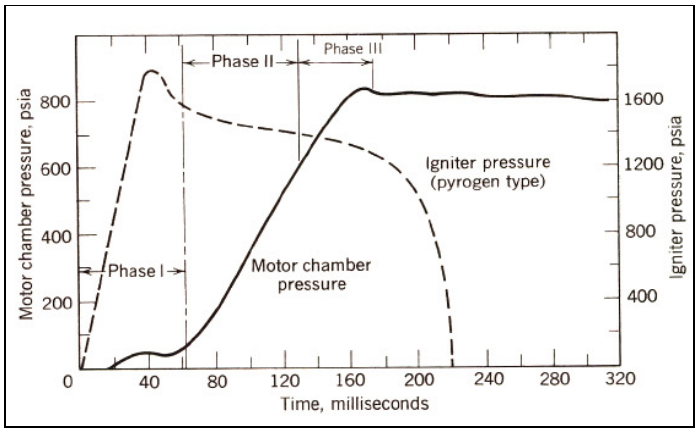

Figure 18. Motor chamber pressure-time profile and igniter pressure-time profile (Sutton & Biblarz, 2001, p525). *The ignition process phases are shown across the two pressure-time profiles. Note that the electrical signal from the ignition controller would be received a few milliseconds before time zero.*

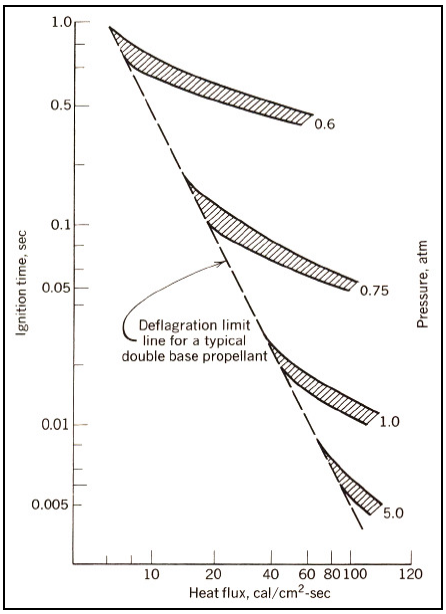

Figure 19. Propellant ignitability curves (Sutton & Biblarz, 2001, p526). *Effect of heat flux on ignition time for a specific motor.*

After viewing the measured thrust-time profiles for some time, it was identified that the slope and shape of the boost phase of each of the motors were very similar; suggesting that variation in the slope from the ignition transient phase to peak thrust was minimal. Because of this, it was deemed that the best way to align the thrust-time profiles without impacting the individual characteristics of the profiles too much was to shift some of the profiles left a small amount, $\Delta t_{correction}$ [s], into negative time values until the boost phase slopes of the motors were in alignment. As this was the final adjustment of the scaled thrust data obtained by the load-cell and DAQ system, the equation used to adjust the thrust-time data into a useful form for comparison with the published Estes profiles came to:

$$F_T(t) = (g_0/1000)(f(t) - (m_0 - \dot{m}(t + \Delta t_{correction}))) - C \qquad (15a)$$

Note that equation 15a superseded equation 15 as the data-adjustment equation. Applying equation 15a to all of the scaled thrust data obtained for phase one of the thesis project yielded the thrust-time profiles for the C6-0 and D12-0 motors displayed in Figures 20 and 21 respectively. The individual thrust-time profiles of the C6-0 and D12-0 motors, including the unadjusted, scaled thrust data plots, can be found in Appendix K.

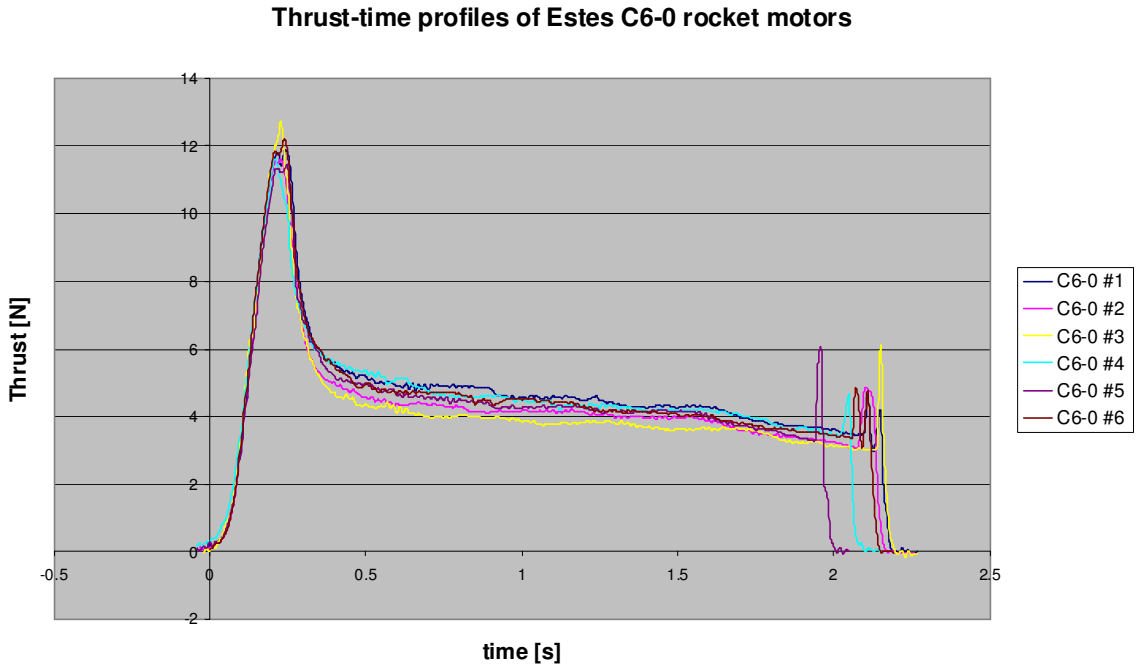

Figure 20. C6-0 thrust-time profiles. *These thrust-time profiles of the C6-0 rocket motors fired in the refined version of the thrust-measuring instrument are the profiles to be used for comparison with the published Estes profiles. If there were errors present in the experiment setup, the errors are common across the population of C6-0 motors tested as the profiles of the motors are very similar.*

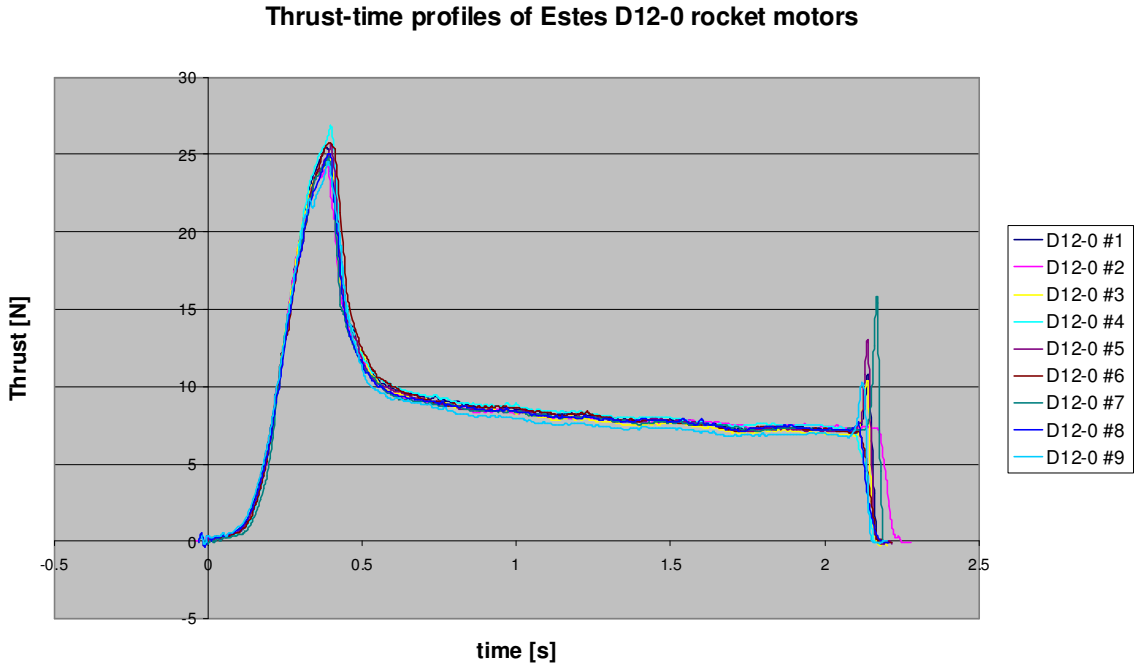

Figure 21. D12-0 thrust-time profiles. *These thrust-time profiles of the D12-0 rocket motors fired in the refined version of the thrust-measuring instrument are the profiles to be used for comparison with the published Estes profiles. If there were errors present in the experiment setup, the errors are common across the population of D12-0 motors tested as the profiles of the motors are very similar.*

2. *Analysis and Comparison of Motor Performance Results*

At a quick glance of the measured thrust-time profiles for both the C6-0 and D12-0 motors, it is immediately obvious of four stand-out differences compared with the thrust-time profiles claimed by Estes in their product catalogue (Figure 3). Firstly, the motors have a longer burn time than what the Estes catalogue claims which suggests that the propellant burn rate is in fact slower than what Estes has measured. Secondly, the maximum

boost thrust is 10% to 20% lower than what the catalogue suggests. Thirdly, there is a sudden spike in thrust just before the motors ceased burning which is not indicated in the Estes catalogue. This phenomenon is very puzzling as the putty end-caps did not allow any gases to escape through the capped-ends of the C6-0 and D12-0 motors which happened during the initial motor trials (refer to Appendix H), thus, generating a reaction force on the load-cell. This suggests that the mass flow rate through the nozzle of the motors increased instantaneously for a very short period of time when the propellant was almost totally consumed. I have identified three possible reasons for this phenomenon. A discussion with A/Prof. Cliff Woodward and Dr. Lynne Wallace of the School of Physical, Environmental and Mathematical Sciences at ADFA yielded the possibility that perhaps the finer particles of the propellant migrated towards the top-end of the motors due to the upside-down orientation at which the motors have been kept while at the hobby shop and in storage. Finer particles would induce a higher burn rate which would increase the thrust for a short period of time. It is also possible that the sulfur burn rate catalyst particles may have accumulated near the top end of the motor during the propellant-packing process, generating a significant spike in thrust at motor burn out. Another possibility for the spike in thrust is that perhaps air-pockets between the rubber propellant seal and the putty end-cap became hot as the burn wave approached, causing the air-pockets to burst, sending pieces of the seal and a rush of hot air up through the nozzle instantaneously increasing the mass flow rate, hence, thrust of the motor. Finally, the measured plateau thrust of the sustainer phase of the motors was neither as constant nor as high as what Estes has claimed in their catalogue. This may be because the clay nozzles of the sample motors actually eroded to a large degree over the burn time due to the high velocity, high temperature exhaust gases (Sutton & Biblarz, 2001, pp555-556). The degree of erosion can be seen in Figure 22. This is another reason why the Estes motors cannot be reused. As the nozzles erode, the nozzle throat area gradually becomes larger which reduces the chamber pressure, hence, reduces the thrust. This would explain the gradual downward slope of the sustainer thrust of the measured thrust-time profiles. It is possible that the nozzles of the motors Estes used to determine the published thrust-time profiles did not erode as much as the nozzles of the sample motors I used, perhaps due to a slightly different clay composition.

Figure 22. Estes motor clay-nozzle erosion. *It is clear from this comparison of a used motor (left) and an unused motor (right) that the exhaust gas flow during firing causes a significant amount of nozzle erosion, particularly at the nozzle throat.*

In order to best compare the details of the measured thrust-time profiles with the thrust-time profiles claimed by Estes (Figure 3), I identified that each thrust-time profile must be characterized by certain identifying key features. The descriptions and values of these characteristic features were tabulated in Appendix L for each individual sample motor, but, also for the published motor thrust-time profiles. It was assumed that the measured values of these characteristic profile features for the six C6-0 and nine D12-0 motors tested were representative of the entire population of these sizes of Estes motors. This assumption allowed me to take the sample means, $\bar{y}$, and the sample standard deviations, s, of the various profile features as being equal to the population means, μ, and population standard deviations, σ, respectively. The equations used to determine the sample mean and standard deviation can be found as equations 16 and 17, respectively.

$$\bar{y} = \mu = (\sum y_i)/N = (y_1 + y_2 + y_3 + \ldots + y_n)/N \tag{16}$$

$$s = \sigma = \sqrt{\text{Variance}} = \sqrt{s^2} = (\sum (y_i - \bar{y})^2)/(N - 1) \tag{17}$$

where y_i is the value of a particular profile feature for the i^{th} motor and N is the number of motors in either the C6-0 or D12-0 sample (Spiegel & Liu, 1999, pp205-207).

It was also assumed that the population distributions of these profile features followed a normal distribution. Because of this assumption, I plotted the profile feature distributions across a spread of values in the range $\mu \pm 3\sigma$; where $\mu \pm 3\sigma$ represents the 99.7% confidence interval, $\mu \pm 2\sigma$ represents the 95% confidence interval and $\mu \pm 1\sigma$ represents the 68% confidence interval (Spiegel & Liu, 1999, p263). By doing this, it enabled me to determine in which confidence interval, if any, the Estes-published value for a particular thrust-time profile feature was included, thus, comprehensively comparing the measured thrust-time profiles with the published

thrust-time profiles of the C6-0 and D12-0 motors. For most of the profile feature distributions, the 99.7% confidence interval of measured results was either far below or above the published value of each profile feature (refer to Appendix L). The only instances where the Estes-published value came close to the measured sample mean was for C6-0 total impulse (shown in Figure 23) and the C6-0 propellant mass (refer to Appendix L). After viewing the sample distributions of the various thrust-time profile features in Appendix L, it is clear that measuring a larger sample of motors (nine D12-0 motors as opposed to only six C6-0 motors) produces a more evenly distributed spread that more closely resembles a normal distribution. The extra reliability gained from using three extra motors in the D12-0 sample was certainly worth the extra cost. This fact should be considered by anyone conducting a similar analysis in the future.

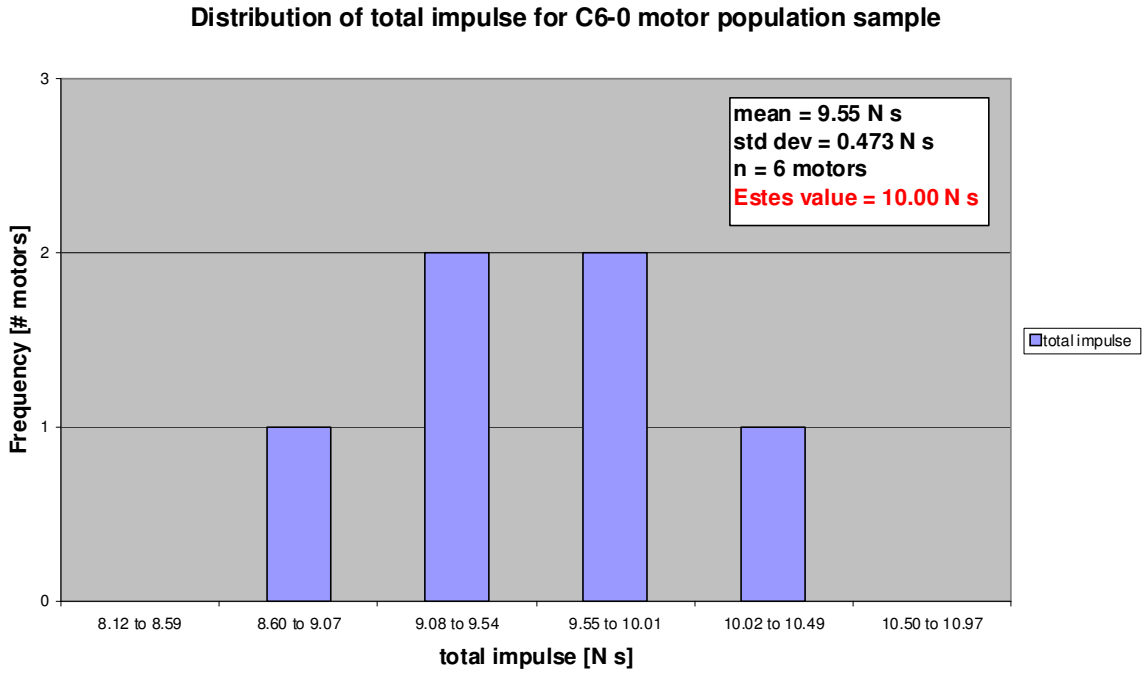

Figure 23. 99.7% confidence interval for measured C6-0 total impulses. *Note that the published value for C6-0 motor total impulse (10 N s) is within the 68% confidence interval of the sample mean (9.55 N s).*

It has been suggested by a number of people that the discrepancies between the measured thrust-time profiles and the published thrust-time profiles (Figure 3) may be due only to *dynamic response errors* in the thrust-measuring instrument. These people suggested that perhaps the relatively high inertia of the steel hinged-cantilever beam caused a delay in the system such that the strain measured by the load-cell at the point of max boost thrust was not truly representative of the actual max boost thrust. They explained that the high inertia of the beam may have reduced the acceleration of the beam towards the point of max deflection enough such that the beam could not 'keep up' with the period of the motors' boost phase (approx 0.6 s to 1.0 s as displayed in Appendix L). Considering that the 250 N XTRAN load-cell has a deflection of 0.013 mm or 13 micrometers at maximum load (250 N) according to the Applied Measurement Australia data sheet on XTRAN 'S'-type load-cells, it seems very unlikely that this suggestion is true. Also, this suggestion may explain why the max boost thrust for the measured thrust-time profiles is lower than for the published thrust-time profiles; however, it fails to explain any of the other discrepancies especially that of total burn time and average sustainer thrust whose distributions are displayed in Figure 24 and Figure 25 respectively.

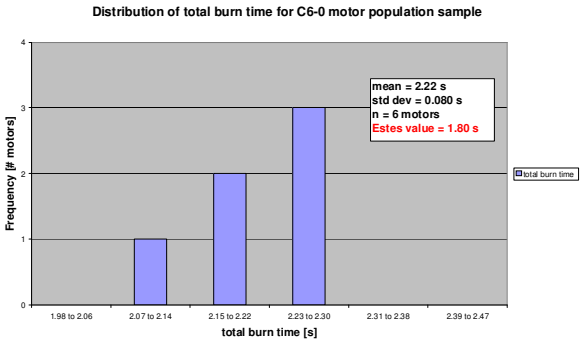
Distribution of total burn time for C6-0 motor population sample
mean = 2.22 s
std dev = 0.080 s
n = 6 motors
Estes value = 1.80 s
Frequency [# motors]
total burn time [s]
1.98 to 2.06
2.07 to 2.14
2.15 to 2.22
2.23 to 2.30
2.31 to 2.38
2.39 to 2.47
total burn time

Figure 24. 99.7% confidence interval for measured C6-0 total burn times. *Note that the published value for C6-0 motor total burn time (1.80 s) is much lower than 99.7% confidence interval of the sample mean (2.22 s).*

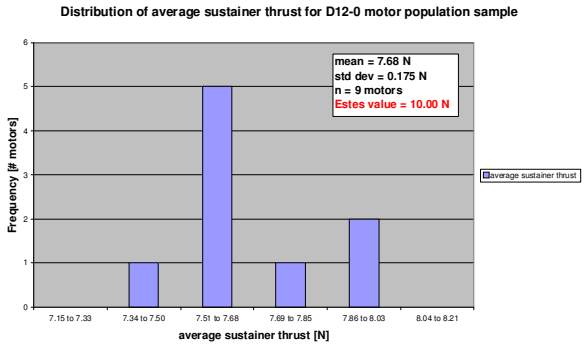
Distribution of average sustainer thrust for D12-0 motor population sample
mean = 7.68 N
std dev = 0.175 N
n = 9 motors
Estes value = 10.00 N
Frequency [# motors]
average sustainer thrust [N]
7.15 to 7.33
7.34 to 7.50
7.51 to 7.68
7.69 to 7.85
7.86 to 8.03
8.04 to 8.21
average sustainer thrust

Figure 25. 99.7% confidence interval for measured D12-0 average sustainer thrusts. *Note that the published value for D12-0 motor average sustainer thrust (10.00 N) is much higher than the 99.7% confidence interval of the sample mean (7.68 N).*

It is quite feasible that the thrust-time profiles of the C6-0 and D12-0 motors that I measured are in fact reliable and that perhaps the motors I purchased for this project are in fact representative of only a small portion of the motor populations. It is also possible that the motors I measured may have been in storage for a very long time such that the motors' propellant grains had undergone certain chemical changes that decreased the propellant burn rate (Sutton & Biblarz, 2001, p464), thus, increasing the total burn time as seen in Figure 24 and Appendix L. The most likely chemical aging process that black-powder would undergo is extensive moisture absorption from the atmosphere as mentioned in Section II, Part C of this report. Another possible explanation for the discrepancies in the measured and published thrust-time profiles is that perhaps the published thrust-time profiles are for motors undergoing the sort of longitudinal accelerations achieved by actual Estes model rockets. As mentioned in Section II, Part C of this report, solid-propellant rocket motors experiencing a longitudinal acceleration will exhibit an increase in burning rate (Fuchs, Peretz & Timnat, 1982, p539). If indeed Estes conducted dynamic motor tests to determine their published thrust-time profiles, it would explain the higher boost and sustainer thrusts and shorter burn times compared with the thrust-time profiles I measured from static tests.

IV. Phase Two — Determining the Temperature Sensitivity of Estes Motor Performance

The second phase of the thesis aimed to determine the temperature sensitivity of Estes solid-propellant rocket motor performance. The size of Estes motor used for this phase of the thesis was the D11-P motor. This motor was used as it was found that it has better resilience to the freezing temperatures used in the temperature sensitivity analysis due to reasons discussed later in this report. The temperature sensitivity analysis of D11-P motor performance was conducted to determine how initial propellant temperature (before ignition) affects the thrust-time profiles of these motors. Amateur model rocket enthusiasts could potentially store then launch their small, black-powder rocket motors in locations here on Earth that could be at temperatures in the range of -30°C to +50°C. It is therefore useful for them to know how the storage temperature will affect the performance of their rocket motors. This sort of analysis also has many military applications. High-performance military solid-propellant missiles/rockets could be launched after storage periods at temperatures within a similar range. The storage temperature of the missiles/rockets will affect their trajectories during operation. Results from this experimentation have been qualified using rocket theory and quantified using calculations. The temperature sensitivity of the black-powder propellant used in the Estes motors has been compared with typical values for commonly used propellants in other commercially-manufactured motors.

A. Temperature Sensitivity Experiment Method

1. Selecting the Storage Temperatures

In order to obtain various initial propellant temperatures for the temperature sensitivity analysis of the D11-P motor performance, the motors used in the analysis each had to be stored at a particular temperature. It was identified that for this analysis to be realistic and worthwhile, only likely Earth-bound motor storage temperatures were selected. -30°C was identified as a typical extreme cold temperature for this analysis as countries at similar latitudes to Russia experience these sorts of temperatures in their winter (Ashcroft, 2001, p149). An environmental chamber (Figure 26) owned by SACME was available for this thesis for one week. This environmental chamber had the capability of generating temperatures as low as -40°C, so achieving -30°C was not a problem (refer to Figure 25). +50°C was identified as a typical extreme hot temperature for this

analysis as arid, desert-ridden countries such as Australia and Iraq, can potentially generate such temperatures (Ashcroft, 2001, p105). Air temperatures of around +50°C can easily be generated near ground level in such countries, especially over air-force-base tarmac, where there could potentially be an AIM-9 missile awaiting fitment to a fighter jet. SACME was able to provide a drying oven (Figure 27) for this thesis for a five day period. The drying oven was set to +50°C. It was identified that having a third 'batch' of motors at a temperature somewhere between -30°C and +50°C would provide for a more accurate determination of the temperature sensitivity of D11-P motor performance as it would provide three data points rather than just two. For reasons of convenience, the third temperature chosen for this analysis was 'room temperature' inside the SACME air-conditioned office of Dr. Milthorpe. The variation in temperature inside his office was measured by Dr. Milthorpe for a period of five days using a max-min thermometer. It was found that the temperature inside the office fell to a minimum of 18.5°C at night and rose to a maximum of 22.5°C during the day. The average temperature over the 5 day period was taken to be 21°C. The room temperature records can be found in Appendix M.

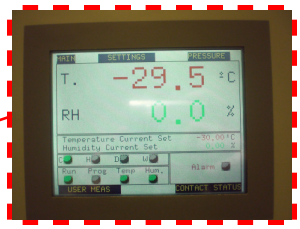

Environmental chamber settings display.

Figure 26. Environmental chamber. *This chamber is owned and operated by SACME. It can generate temperatures between -40°C and +180°C and even has a relative humidity (RH) setting option. It maintained -30±1°C for the 7 day period the motors were being stored.*

Figure 27. Drying oven. *This oven is owned and operated by SACME. It maintained +50±1°C for the 5 day period the motors were being stored.*

2. Storage Time Period

In order to achieve reliable results for the temperature sensitivity analysis, it was identified that the D11-P motors used in the analysis had to be stored at the selected temperatures (-30°C, +21°C and +50°C) for a long enough period of time to ensure that the entirety of the propellant grain had reached that chosen temperature. Due to the fact that the thermal conductivity of black-powder was very difficult to find, it was assumed that the thermal conductivity of black-powder is approximately the same as for anthracite coal, which is 0.26 W m^{-1} K^{-1} (Incropera, DeWitt, Bergman & Lavine, 2007, p939). This assumption was made because coal has a similar chemical composition to black-powder (Zondlo & Velez, 2007, p370) but it also has a similar density with the compacted black-powder used in the Estes motors which I calculated to be approx. 2000 kg m^{-3} (refer to Appendix O). Anthracite coal has a density of approx. 1350 kg m^{-3} (Moran & Shapiro, 2004, p793). As this thermal

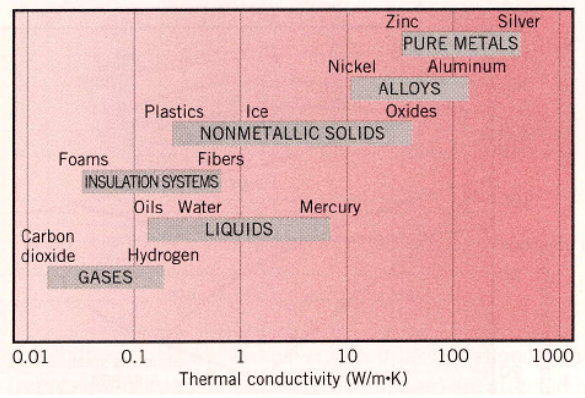

Figure 28. Range of thermal conductivity for various states of matter at normal temperatures and pressures (Incropera, DeWitt, Bergman & Lavine, 2007, p61).

conductivity is quite low and is of the same magnitude as some insulating materials (refer to Figure 28), it was identified that the motors would have to be kept at the chosen storage temperatures for as long as practically possible to ensure that the motor propellant grains were uniformly saturated at the desired temperature. The 'cold' batch of motors, consisting of four D11-P, one C6-0 and one D12-0, were left in the environmental chamber at -30°C for 7 days. The 'room temperature' batch of motors, consisting of three D11-P, one C6-0 and one D12-0, were left in Dr. Milthorpe's office for 5 days. The 'hot' batch of motors, consisting of three D11-P, one C6-0 and one D12-0, were left in the drying oven at +50°C for 5 days. Note that at this stage of phase two of this thesis project, it was intended to obtain the temperature sensitivity of the remaining C6-0 and D12-0 motors left over from phase one, as well as the D11-P motors. For reasons mentioned later in this report, this was not possible.

3. Firing the Rocket Motors

On the final day of storage, the motors were to be fired in the thrust-measuring instrument in order to obtain the thrust-time profiles. It was identified that the moment the motors were extracted from their temperature-controlled environment, the propellant would either start heating up or cooling down, depending on whether the propellant temperature was lower or higher than the ambient temperature, respectively (Incropera, DeWitt, Bergman & Lavine, 2007, pp4-11). In an effort to reduce the undesired temperature change in the propellant, a strategy was implemented for the motor firing experiment. Instead of setting-up the thrust-measuring instrument in the courtyard outside the SACME welding bay, which is a considerable distance from the environmental chamber and drying-oven, the instrument was set-up directly outside the building containing the chamber and oven. The experiment was setup to a point where the only thing left to do was insert a motor into the thrust-measuring instrument, apply the motor restraint, install the igniter fuse, begin saving the data and then press the ignition switch. At this point, I would go to either the environmental chamber or drying-oven to fetch a single motor, install the motor in the instrument without delay, and fire it. As Dr. Milthorpe's office was a long distance from where I was conducting the experiment, the 'room temperature' batch of motors was kept inside my bag, wrapped in cloth for added insulation. As the temperature difference between the 'room temperature' motors and the ambient air temperature was relatively small, the heat loss from the motor propellant was not considered to be a major problem (Incropera, DeWitt, Bergman & Lavine, 2007, pp4-11).

4. Thrust-Measuring Instrument Design Flaw

Once all of the D11-P motors were fired and their thrust-time profiles obtained, a 'cold' D12-0 motor was inserted into the thrust-measuring instrument and fired. Unfortunately, the motor exploded which created a large enough force to destroy the 250 N XTRAN load-cell. The maximum load of 250 N was exceeded by a considerable amount which caused the load-cell to buckle and deform. This incident rendered the load-cell completely useless. Fortunately, however, the motor-holder cup contained the motor case from splitting apart which may have distributed shrapnel radially outwards. After much thought, a hypothesis on what caused the motor to explode was reached. It is possible that the thin, weak end-seal of the D12-0 motor allowed moisture to seep into the black-powder grain considering that black-powder is very hygroscopic. This moisture may have come from the atmosphere or from the wet water-based putty used to reinforce the end-seal (as discussed in Section III, Part A, Subsection 2). If the propellant did indeed contain pockets of water moisture, then as the propellant was brought to below-0°C temperatures inside the environmental chamber, the moisture pockets would have frozen. It is a well known fact that as water freezes, it expands. As the frozen moisture expanded inside the propellant grain, it would have caused localized tensile stresses on the grain. If these localized tensile stresses were large enough, they would have caused the brittle black-powder propellant grain to crack, thus, exposing a greater exposed surface area. After motor ignition, the burn wave would have propagated towards the crack/s in the grain. Providing the cracks were large and deep enough, the large increase in the exposed surface area of the grain would have increased the chamber pressure to the point where the case became overpressurized (Sutton & Biblarz, 2001, p454). The path of least resistance for the excess pressure to break out of the motor case was to blow the nozzle and remaining propellant out of the motor case into the air. The sudden expulsion of mass upwards (both nozzle and propellant) generated a large enough force downwards to overload and deform the load-cell.

Another 'S'-type load-cell was available to this thesis project, albeit a 350 N maximum allowable load instead of 250 N. The 350 N load-cell was the same dimensions as the 250 N load-cell that was destroyed. This meant that I was not required to significantly modify the thrust-measuring instrument to fit the new load-cell. As the XTRAN load-cells are relatively expensive (approx. AU$400.00), I identified the need for an overload-protection modification to the thrust-measuring instrument. Considering the time constraints of the thesis project, I devised a simple yet effective system of ensuring that if another motor exploded, the load-cell would not be destroyed. The overload-protection system consisted of a 10 mm diameter nut welded to the base plate of the instrument directly under the hinged-cantilever beam with a 70 mm long bolt screwed into the nut the required amount. The method of operation of this system involved selecting a limit load that was well under the

limit load of the load-cell (350/4=87.5 N) but well over the maximum thrust expected from the motor (30 N). I used 50 N (approx. 5000 g) at the motor-holder cup which was amplified to 200 N at the load-cell. During the calibration of the instrument, the beam would be loaded-up with a 5000 g weight. The bolt would then be unscrewed from the welded nut until the head of the bolt came in contact with the underside of the beam. A lock-nut which was already threaded onto the bolt would then be tightened against the welded nut to prevent any movement in the finely adjusted position of the bolt. The 5000 g weight was removed and the instrument was calibrated as normal. This overload-protection system proved to be very effective. It did not interfere with the measured thrust values of the motors as the motors did not produce enough thrust to strain the load-cell enough for the underside of the hinged-cantilever beam to come into contact with the bolt. However, if a load greater than 50 N was applied at the motor-holder cup position (i.e. if a motor exploded again), the beam would strain the load-cell until the underside of the beam came into contact with the bolt. At this load-cell strain position, the bolt would take up the remaining load without straining the load-cell any further, thus, protecting the load-cell from being deformed. Because of this, an overload of the instrument (>50 N) would only register as a 50 N load by the load-cell. The calibration check displayed in Figure 14 was conducted with the overload protection system in place. At time t=24 s, a 7000 g weight was applied to the instrument to ensure the correct operation of the overload protection system. Note that the measured load only increased a very small amount above the 5000 g limit imposed on the instrument. The overload-protection system can be seen in Figure 29.

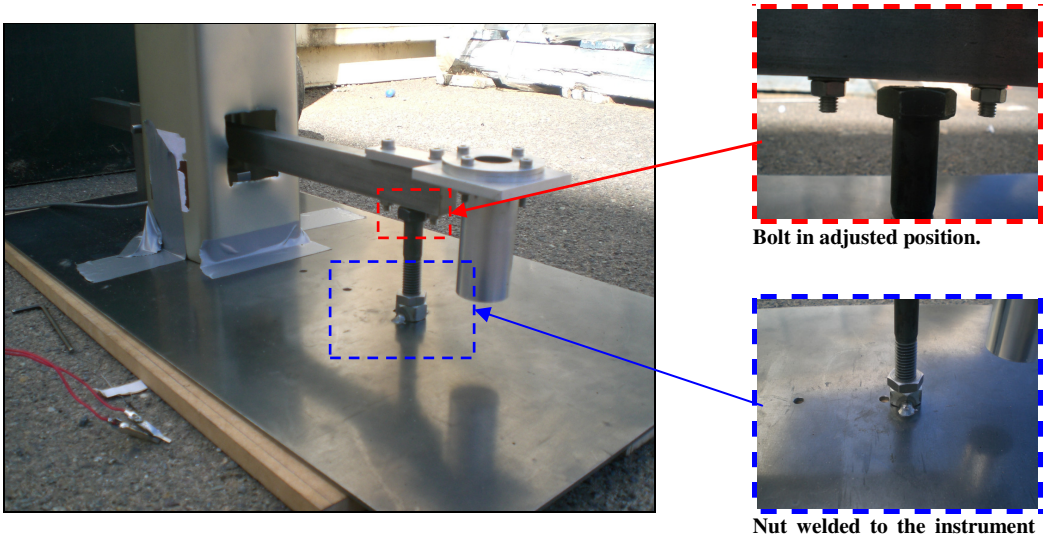

Figure 29. Load-cell overload protection system. *If the motor inside the motor-holder cup was to explode or generate a thrust that would exceed the limit load of the load-cell, the bolt would contact the underside of the beam, hence, the bolt would support the excess load rather than the load-cell supporting the entire load.*

B. Analysis of Temperature Sensitivity Results

1. Collection and Presentation of Measured Results

Equation 15a was applied to the scaled thrust data obtained for phase two of the thesis project for the same reasons identified in Section III, Part A, Subsection 5 of this report. The plotted results can be seen in Figure 30. The individual thrust-time profiles for the D11-P motors, including the unadjusted, scaled thrust data plots, can be found in Appendix N.

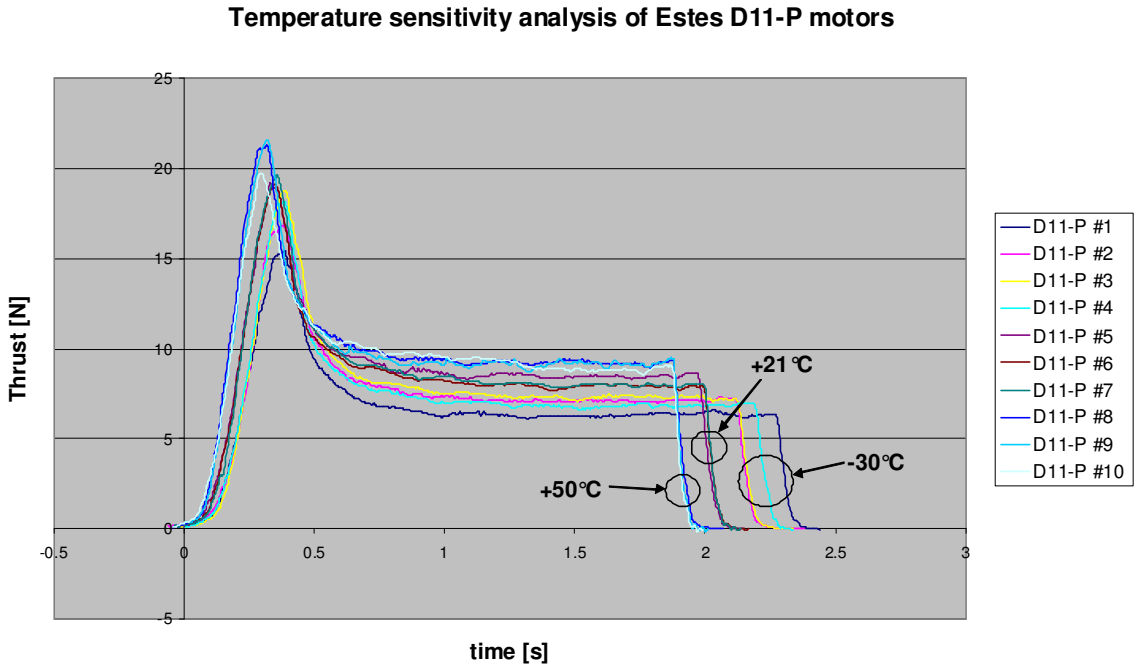

Figure 30. Thrust-time-temperature profiles of the Estes D11-P motors. *Even though there is some variation in the thrust-time profiles within each 'temperature' batch of the D11-P motors, it is rather evident that initial propellant temperature affects the performance of solid-propellant rocket motors as expected from the trend displayed in Figure 6.*

It was anticipated that there would be a greater degree of variation in thrust-time profiles within each 'temperature' batch of motors than for phase one of the thesis project because an extra variable, initial propellant temperature, was included in the experiments. This was the reason why I elected to fire at least three D11-P motors for each of the selected storage temperatures. As explained earlier in the report, testing a larger sample of D11-P motors at each temperature would have provided a better representation of the overall population spread and mean of the D11-P thrust-time-temperature profiles but other factors such as cost, time and motor availability must be considered. As the aim of this phase of the thesis was to compare the thrust-time profiles of the D11-P motors across different initial propellant temperatures, it was decided that the best way to display the results was to average the thrust-time profiles of the motors from each 'temperature' batch and then plot the three averaged profiles on the same graph. It was decided that the best way to average the thrust-time profiles was to average the thrust values across the longest burn time within each batch. This simply involved summing the thrust values at the i^{th} time value, $F(t_i)$, across each batch and dividing by the number of motors in the batch, b, or:

$$F(t_i)_{avg} = \sum F(t_i)/b \tag{18}$$

The averaged thrust-time-temperature profiles of the D11-P motors fired during phase two of the thesis are displayed in Figure 31.

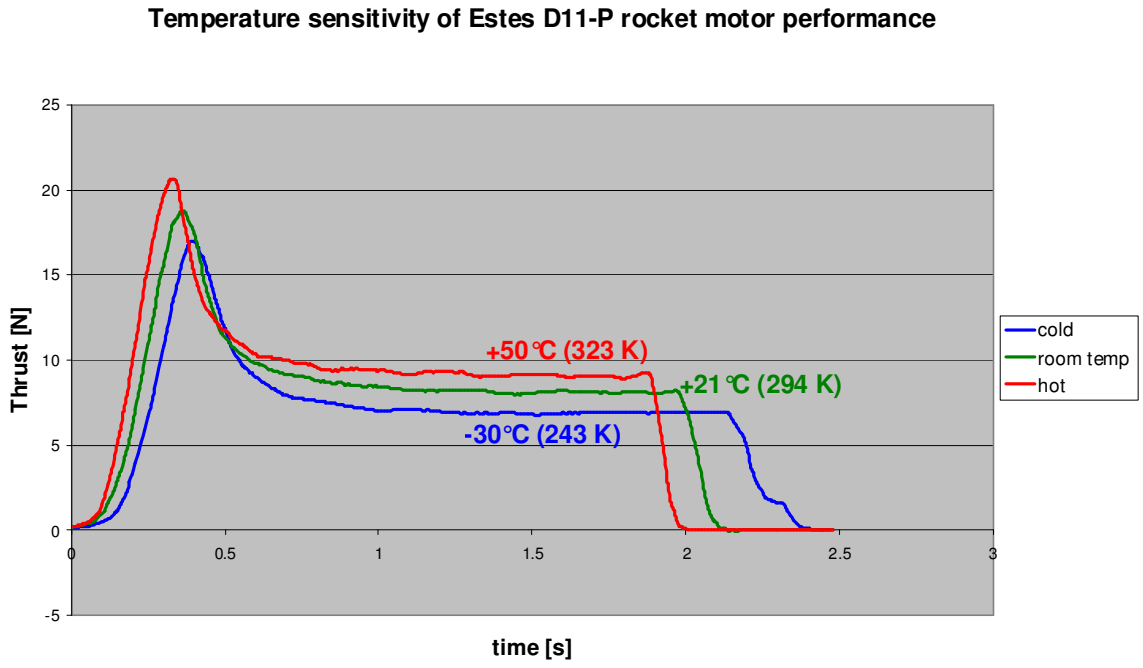

Figure 31. Averaged thrust-time-temperature profiles of each 'temperature' batch of D11-P motors. *The values for chamber pressure required to calculate the temperature sensitivity of pressure for the D11-P motors were calculated from the average thrust values of these thrust-time-temperature profiles. From this plot it is easy to see that the temperature trend matches the expected trend from Figure 6.*

2. *Analysis of the Results*

It was assumed that the propellant burn rate, r, propellant exposed burning surface area, A_b, and nozzle throat area, A_t, were relatively constant over the burn time of the end-burning Estes rocket motors. Because of these assumptions, temperature sensitivity of burn rate, σ_p, could not be calculated but temperature sensitivity of chamber pressure, π_K, could be calculated for constant motor geometry, K (refer to equation 11). To determine a value for the temperature sensitivity of D11-P motor performance, equation 10 was applied to the average thrust-time-temperature profiles displayed in Figure 31. To calculate the chamber pressure, p, of each averaged thrust-time-temperature profile from Figure 31, it was necessary to average the thrust across the entire burn time for each profile. Using the method explained in Appendix O, the averaged parameters for each batch of D11-P motors tabulated in Table 1 were entered into the rocket design MATLAB code (Appendix O) which outputted a value for the average chamber pressure for each averaged profile. The values in Table 1 were plotted in Figure 32. As $\pi_K=(\partial \ln p/\partial T_0)_K$, the gradient of the line-of-best-fit for the plotted values gave the value of π_K for the Estes D11-P rocket motors.

Temperature batch	Temperature [℃]	Average thrust [N]	Total impulse [N s]	Burn time [s]	Average chamber pressure [Pa]	Natural log of chamber pressure (ln p[Pa])
cold	-30	6.59	16.41	2.40	487000	13.096
room temp	21	8.08	17.69	2.14	573000	13.259
hot	50	8.93	18.75	2.02	622000	13.341

Table 1. Averaged parameters for each 'temperature' batch of D11-P motors. *These values were determined from the data displayed in Figure 31. The chamber pressures were calculated by inputting the respective average thrust, total impulse and burn time values into the rocket_design MATLAB code (Appendix O) which outputted the value for chamber pressure, p_1, for each batch of D11-P motors.*

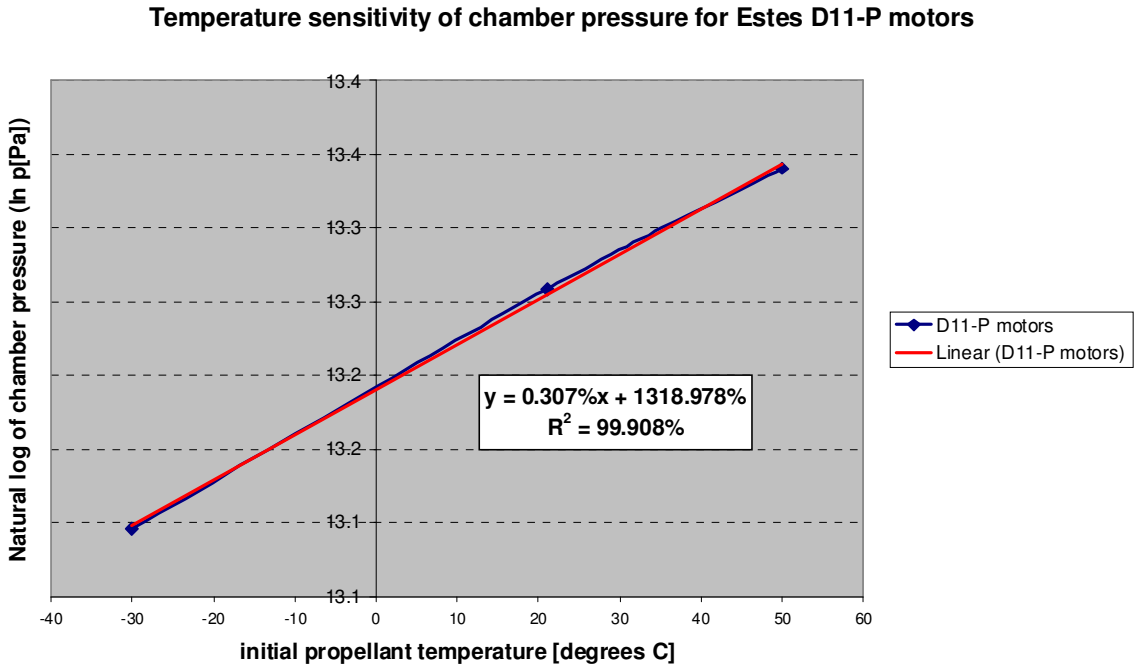

Figure 32. Temperature sensitivity of D11-P motor performance. *This plot displays the relationship between initial propellant temperature and the average chamber pressure (performance) of the D11-P motors tested during phase two of the thesis. The gradient of the linear relationship represents the temperature sensitivity of chamber pressure, π_K [% °C^{-1}], for the Estes D11-P rocket motors.*

From Figure 32, the temperature sensitivity of pressure at constant motor geometry, π_K, was found to be 0.307 % °C^{-1}. Typical values of π_K are 0.067 % °C^{-1} to 0.278 % °C^{-1} (Sutton & Biblarz, 2001, p432). π_K for the black-powder D11-P Estes rocket motors is much larger than typical values of π_K for useful, larger-scale rocket motors. This suggests that initial propellant temperature has a greater affect on the performance of the D11-P motors which is an undesirable trait to have in a solid-propellant rocket motor because it makes it more difficult to calculate missile/rocket trajectories, especially if the rocket motor is exposed to large variations in ambient temperature over its burn time.

V. Phase Three — Designing, Constructing & Testing Home-Made Solid-Propellant Motors

The third or final phase of the thesis was to design, construct and test two home-made solid-propellant rocket motors. The intention was to design two motors with the same performance (total impulse) as the C6-0 and D11-P sizes of Estes motors used in the first two phases of the thesis. A home-made propellant recipe was extracted from Sleeter, 2004, p252. The design of the home-made motors involved applying thermodynamic nozzle theory and by making a number of assumptions about the combustion of the home-made propellant. Finally, the thrust-measuring instrument used in the first and second phases of the thesis project was used to measure the thrust-time profiles of the home-made motors, thus, enabling a comparison with the black-powder Estes motors. Commercially-produced model rocket motors, such as Estes products, are very reliable; however, they are expensive to the amateur model rocket enthusiast (refer to Appendix R), especially considering the motor casing is non-reusable. If a reusable home-made solid-propellant rocket motor could be designed, constructed and launched for a much lower cost than that of the commercially-produced motors while still being competitive in the areas of performance, reliability, safety and convenience, then this home-made motor would be a very attractive alternative to purchasing expensive motors from hobby shops. The thesis succeeded in creating two reusable home-made motors that represent a cheaper alternative to the motors produced commercially, such as the Estes motors; however, more development work is required to match the performance of the home-made motors with the Estes products.

A. Designing the Home-Made Motors

1. The Home-Made Propellant Recipe

Obtaining a home-made solid-propellant recipe was the first step in designing a home-made rocket motor. I identified two requirements for the propellant. One requirement was that the propellant would be easily mixed without the use of specialized mixing equipment due to the tight time constraints of the thesis project. The other

requirement was that the propellant components would be readily available and would be safe to handle with minimal safety precautions. A propellant recipe that satisfied these two requirements was found in Sleeter, 2004, p252, which detailed a propellant recipe for mixing icing sugar (the fuel, seen in Figure 33) with potassium nitrate (the oxidiser, seen in Figure 34) and adding a small amount of baking soda (burn rate modifier, seen in Figure 35). The propellant recipe was designated as the *KS propellant*. The recipe involved adding 60% by weight potassium nitrate (KNO_3) and 40% by weight icing sugar ($C_{12}H_{22}O_{11}$) to a soft plastic container and shaking the container for 2 minutes. 6% baking soda ($NaHCO_3$) was mixed thoroughly into the propellant to reduce the burn rate to avoid motor case overpressurization.

Figure 33. Icing sugar ($C_{12}H_{22}O_{11}$) fuel.

Figure 34. Potassium nitrate (KNO_3) oxidiser.

Figure 35. Baking soda ($NaHCO_3$) burn rate modifier.

2. *Designing the Motor Cases, Nozzles and End-Caps*

As the purpose of this phase of the thesis was only to demonstrate two reusable home-made motors and that the motors were not required to fly in an actual model rocket, the weight of the motors was not considered as a design issue. As the burn characteristics of the KS propellant were largely unknown, I deemed a suitable and safe option to over-engineer the motor cases to ensure that if the KS propellant burnt much faster than predicted, the motor cases would not explode. For strength and ease of machining, the motor cases, nozzles and end-caps were to be made out of common steel. For simplicity and ease of packing the motors with propellant, the motors had a threaded nozzle and end-cap which screwed on to the motor case. This provided easy access to the inside of the motor case and the thread also created a sufficient seal between the nozzle/end-cap and case to contain the chamber pressure.

As the goal of this phase of the thesis was to measure the performance of two home-made motors, it was identified that the home-made motors should exhibit the same case outer diameter as the Estes motors such that the home-made motors could be inserted into the motor-holder cup of the thrust-measuring instrument used in phases one and two of the thesis. As the burn characteristics of the KS propellant were largely unknown, I realized that perhaps the best way to initiate the design of the first home-made motors was to produce two end-burning grain motors that contained the same mass of propellant, m_p, as the C6-0 (m_p=12.48 g) and D11-P (m_p=24.93 g) motors. As the density, ρ_b, of the KS propellant was much less than the density of the Estes black-powder (approx 70%) and the inside-diameters of the motor cases were set to be the same as the Estes motors (the case wall thickness was also the same at 3 mm), the length of the home-made motor cases, L_b, had to be much longer than the Estes motor cases in order to fit the same mass of propellant. It was assumed that the burn rate, r, of the KS propellant was going to be very similar to that of the black-powder used in the Estes motors. Applying equation 8 to determine the mass flow rate, $\dot{m}$, of the motors, I identified that the mass flow rate of the home-made motors was going to be smaller than the mass flow rate of the Estes motors due to the burning surface area, A_b, being the same but the density of the KS propellant being lower. According to equation 5, a lower mass flow rate will result in a lower thrust, F, assuming that the exhaust exit velocity, c, is approximately the same. This meant that in order to produce the same total impulse, I_t, as the Estes motors, the home-made motors would have a longer motor burn time, t_b. All of the above mentioned analysis is detailed in Appendix O.

Applying the thermodynamic theory detailed in Appendix O, a MATLAB code was written to accept nozzle throat diameter, d_t, as an input and to calculate the combustion-chamber pressure, p_1, and temperature, T_1, of the Estes and home-made motors among other parameters. As the nozzle throat diameters of the Estes motors could be measured, the chamber pressure and temperature values of the Estes motors were used as a benchmark for the home-made motors. As the combustion characteristics of the KS propellant were largely unknown at this stage, I assumed that the combustion of the KS propellant would generate the same chamber pressures and temperatures in the home-made motors as the black-powder combustion produced in the Estes motors. Using this assumption, different nozzle throat diameters were inputted for the 'C' size and 'D' size home-made motors

until the MATLAB code outputted similar chamber conditions (p_1 and T_1) as for the Estes C6-0 and D11-P motors respectively. The MATLAB code also outputted a nozzle exit diameter, d_2 [m], the hoop stresses, σ_1 [Pa], and longitudinal stresses, σ_2 [Pa], generated in the motor case wall. The output of the MATLAB code can be found in Appendix O. From this analysis I obtained the required nozzle inlet, throat and exit diameters for both the 'C' size and 'D' size home-made motors. This enabled me to draw the engineering drawings for the home-made motor cases, nozzles and end-caps using the CAD program *PTC ProDESKTOP*. These drawings can be found in Appendix P.

B. Construction of the Home-Made Motors

1. *Constructing the Motor Cases, Nozzles and End-Caps*

The engineering drawings of the 'C' size and 'D' size home-made motor designs were submitted to a workshop for construction. The motors were constructed precisely according to the drawings, however, due to the finicky and small detail contained in the nozzle designs, the nozzle's convergent and divergent sections were slightly off and the surface finish inside the nozzle was probably too rough for near-ideal isentropic flow through the nozzle. More importantly though was that the nozzle inlet, throat and exit diameters were exactly as designed. The finished home-made motors can be seen in Figure 36 alongside the respective Estes motors that they have been modelled off.

Figure 36. Finished home-made motors. *The home-made motors were required to be longer than the Estes motors in order to pack the same mass of propellant into the motor cases due to the KS propellant being less dense than the black-powder. Note that the end-cap and nozzle screw onto the motor case.*

2. *Constructing the Home-Made Ignition System*

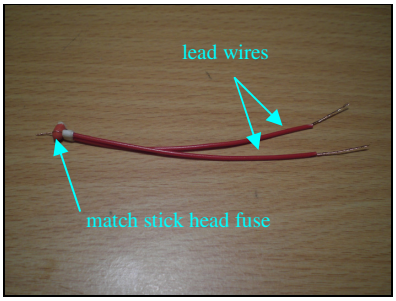

Figure 37. Home-made igniter fuse and leads.

It was pointed out to me that my home-made rocket motors would not be a viable alternative to commercially-produced rocket motors if I did not develop a home-made ignition system. Producing a home-made ignition system, which was based on a system described in Sleeter, 2004, pp456-458, was a matter of trial and error. The final solution I used involved wrapping the ends of two 70 mm-long pieces of thin electrical hook-up wire (leads) around a match stick head (fuse), securing the two pieces of wire together with a small piece of masking tape (Figure 37) and attaching the lead wires to two 5 m-long lengths of thicker electrical wire (ignition wires). The match stick head and lead wires would be poked through the nozzle of the home-made motor and pressed up against the exposed end-burning surface of the propellant inside the motor case. Operating the ignition system involved touching the ends of the thicker electrical wire to the terminals of a 12 V motorcycle battery. The battery would provide enough electrical power to heat up the thin pieces of lead wire around the match stick head until the wire would burn, thus, igniting the match stick head, thus, igniting the home-made propellant.

3. Packing the Motor Cases with Propellant

Before packing the motor case with propellant, the end-cap was screwed onto the motor case and tightened. The nozzle was left off until the ignition system was inserted. As detailed in Sleeter, 2004, p253, a small amount (approx 3 g) of propellant was inserted into the motor case at a time. The tamp, which was made out of wooden dowel rod to prevent any sparks from being generated, was then inserted into the motor case as shown in Figure 39. A few light taps with the hammer on the wooden dowel tamp removed any excess air from the propellant powder. Once this had been conducted, a few solid hammer blows on the tamp compacted the propellant sufficiently into the motor case. This process was repeated until all of the propellant had been compacted into the motor case as shown in Figure 38. According to Sleeter, 2004, p369, once mixed the KS propellant crystals will continue to self-mix, becoming finer and finer until the burn rate increases to a point that might overpressurize the motor case. For this reason, Sleeter recommends to fire the KS propellant motors within 2 days of mixing the propellant. The propellant is also extremely hygroscopic, readily absorbing water from the atmosphere. Once fired, the home-made motors were cleaned out with hot water and repacked with propellant for a second firing.

Figure 38. Home-made motors packed with KS propellant. *The KS powder propellant was white in colour and was compacted to a surprisingly solid substance.*

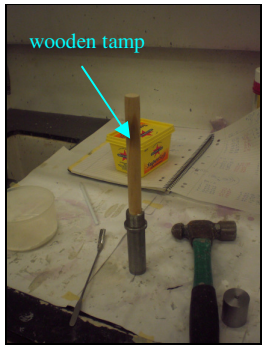

Figure 39. Home-made motor packing process.

C. Testing the Home-Made Rocket Motors

1. Experiment Setup

The experiment setup was exactly the same as the setup detailed in Section III of this report; however, barriers were placed over and around the thrust-measuring instrument in case the steel motor nozzle was shot off the motor case due to an overpressurization. The barriers would prevent the nozzle from becoming a potentially lethal projectile. A wire mesh barrier was placed over the instrument to allow the exhaust plume to flow unimpeded, necessary for reliable thrust results, while being able to contain the nozzle if it did shoot off the motor case. The home-made motors were each inserted into the motor-holder cup of the instrument, the igniter fuse and leads were inserted through the nozzle and hooked up to the longer ignition wires, the data saving was commenced and the ignition wires were contacted onto the terminals of the motorcycle battery. The motors usually ignited without fault.

2. Measured Performance of the Home-Made Motors

Equation 15a was applied to the scaled thrust data obtained for phase three of the thesis project for the same reasons identified in Section III, Part A, Subsection 5 of this report. The thrust-time profiles of the 'C' size and 'D' size home-made motors are displayed in Figures 40 and 41. I have identified the home-made motors as C6.5 and D11.5 motors in order to distinguish them from the Estes motors. Once fired, the home-made motors were cleaned out with hot water, repacked with propellant and then fired a second time, thus, demonstrating their reusability. The individual thrust-time profiles of the home-made C6.5 and D11.5 motors, including the unadjusted, scaled thrust data plots, can be found in Appendix Q.

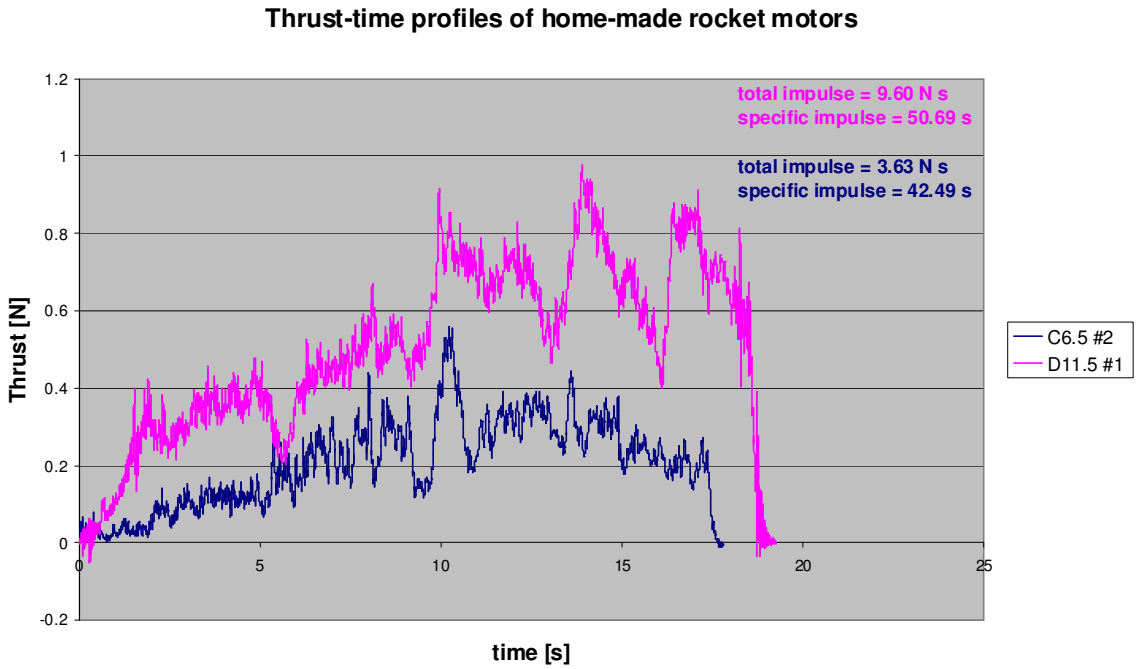

Figure 40. Thrust-time profiles of home-made motors. *These thrust-time profiles of the home-made rocket motors fired in the thrust-measuring instrument are examples of what happens when combustion instabilities occur in the combustion-chamber of solid-propellant rocket motors. These profiles show that the home-made motors only generate a fraction of the thrust produced by the Estes motors, but they burn for a much longer time.*

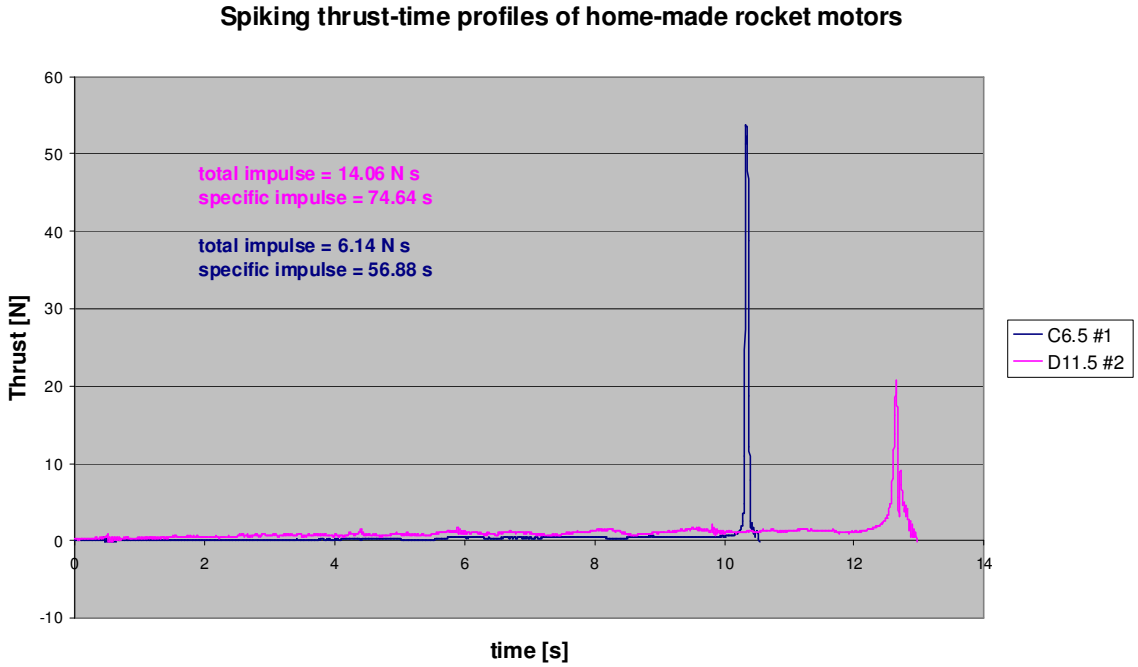

Figure 41. 'Spiking' thrust-time profiles of home-made motors. *These thrust-time profiles of the home-made rocket motors fired in the thrust-measuring instrument are examples of what happens when a large amount of propellant inside the motor case combusts all at the same time. It generates a large instantaneous mass flow rate which causes a spike in thrust.*

3. Analysis of Measured Results

At a quick glance of the measured thrust-time profiles of the home-made motors, four characteristics are immediately obvious. Firstly, the burn times of the motors are much longer than that of the Estes motors. This suggests that the burn rate of the KS propellant is in fact much slower than black-powder used in the Estes motors. Considering equation 7, perhaps the burn rate, r, was much lower than the burn rate of the Estes motors because the combustion-chamber pressure, p_1, was not able to reach the chamber pressures obtained in the Estes motors for various reasons. In an attempt to increase the burn rate of the KS propellant, no $NaHCO_3$ burn rate modifier was added and also the KNO_3 powder was milled into a finer powder using a powder mill (shown in Figures 42 and 43) for the second lot of home-made motor firings (C6.5 #2 and D11.5 #2 in Figures 40 and 41). Decreasing the particle size of the oxidiser should have increased the burn rate of the KS propellant. This appeared to have happened to a small extent for the D11.5 motor but not for the C6.5 motor. Secondly, a spike in the thrust of the first C6.5 and second D11.5 motor can be seen in Figure 41. It is believed that because the burn time of the motor was much longer than expected, the heat generated by the combustion of the KS propellant caused the steel case of the motors to heat up to the auto-ignition temperature of the propellant. As the heat transfer rate through the steel would be quite high (high thermal conductivity as seen in Figure 28), it seems that once the steel around the remaining, unburned propellant reached the auto-ignition temperature, the remaining propellant combusted all at once, generating an extremely high chamber pressure, mass flow rate and, therefore, high thrust. Fortunately, the load-cell overload protection system saved the load-cell from being destroyed. Figure 44 displays the high exhaust mass flow rate during one of these spikes in thrust. Thirdly, the thrust produced by the home-made motors was much lower than the Estes motors. This was due to the fact that the burn rate, hence, mass flow rate of the home-made motors was much lower than predicted. Finally, the combustion of the KS propellant looks to be very unstable as the thrust generated is not smooth and relatively constant. This *combustion instability* is caused by pressure oscillations inside the combustion-chamber that may be caused by large particles in the exhaust gases partially blocking off the nozzle throat (Sutton & Biblarz, 2001, pp528-532). As the combustion of the KS propellant was found to generate a lot of soot and is a rather crude propellant, this seems to be the most likely reason for the combustion instabilities.

Figure 42. Powder mill drum with ball pellets.

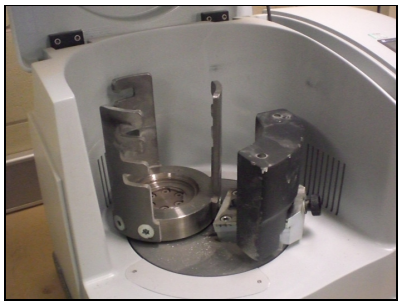

Figure 43. Powder mill spinner.

Figure 44. Spike in thrust of the C6.5 home-made motor. *From this snapshot of a motor firing, it is evident that the mass flow rate is very high from the opacity of the exhaust plume, hence, large amount of matter in the exhaust flow. This was caused by a large amount of propellant combusting all at once.*

The total impulses achieved by the home-made motors were much lower than what the motors were designed to achieve. This is due to the fact that the burn rate, hence, mass flow rate was much lower than predicted. The total impulses for the four firings of the home-made motors are displayed in Figures 40 and 41. As the dimensions of the home-made and Estes motors were very similar, the specific impulses of each provide a good comparison of KS propellant performance with black-powder performance. From the specific impulse values, it appears that the KS propellant has much less performance than the black-powder propellant used in the Estes motors. The average specific impulses of the KS propellant and black-powder propellant were 56.2 s and 76.5 s respectively. According to Sutton & Biblarz, 2001, pp424-425, typical specific impulses for commercially-produced, high performance missile and space motors are 250 s to 300 s, much larger than the small model rocket motors used in this thesis project. The propellant mass fractions, ζ, of the Estes motors were far higher than ζ for the home-made motors due to an efficient, high thrust-to-weight design of the Estes motors.

This is because the mass of the home-made motors was not optimised for flight due to the reasons detailed in Section V, Part A, Subsection 2. The value of ζ for the Estes C6-0 and D11-P motors is 0.55 and 0.57 respectively, as calculated from the published values in the Estes product catalogue (Estes Catalogue, 2006, p35). The average value of ζ for the home-made C6.5 and D11.5 motors is 0.035 and 0.048 respectively.

VI. Conclusions

This thesis project developed a very effective, simple and reliable method of measuring the thrust-time profile of a small solid-propellant rocket motor. This thrust-measuring instrument was applied to confirm the published thrust-time profiles of C6-0 and D12-0 size Estes model solid-propellant rocket motors detailed in their product catalogue. The results showed that the thrust-time profiles of these motors may in fact not be as Estes Industries claim, albeit quite close. The thrust-measuring instrument was further applied to determine the effect that initial propellant temperature has on the performance of the D11-P size Estes model rocket motors. It was found that initial propellant temperature affects the performance of the Estes black-powder motors to a greater extent than other commercially-produced rocket motors. This is certainly one of the many reasons why black-powder is no longer used as a propellant in contemporary rocket motors other than in amateur model rocket motors. This thesis culminated in the development and testing of two home-made, solid-propellant rocket motors. Results from testing the home-made motors revealed that it is very difficult indeed to develop a small rocket motor that has a similar performance to commercially-produced motors such as the Estes motors. This fact is understandable considering that Estes Industries has had 50 years experience in producing small model rocket motors for amateur model rocket enthusiasts. This thesis project has provided me with a very broad understanding of the engineering and science behind solid-propellant rocket motors. I hope that the readers of this final thesis report learn something interesting about solid-propellant rocket motors, which are a very useful, simple and inexpensive method of propulsion. For anyone who wishes to continue my work in the area of solid-propellant rocket motors, it is a very fun and enjoyable thesis topic.

VII. Recommendations

Future work in the area of solid-propellant rocket motors should continue to explore the design, construction and testing of home-made rocket motors. Designing, constructing and testing a home-made rocket motor provides an overall, generalized knowledge of solid-propellant rocket motors which would greatly benefit anyone in the ADF. This would be far more beneficial to the person conducting the work than exploring a specific area of solid-propellant rocketry. The work I initiated in phase three of the thesis project should be continued to improve the performance of the home-made motors. Future improvements could involve varying the motor dimensions and materials, varying the propellant fuel to oxidiser ratio and particle size, varying the geometry of the propellant grain, varying the type of propellant used and/or optimizing the thrust to weight ratio of the home-made motor for launch in an actual model rocket motor. How ever the work is continued, I strongly recommend that the thrust-measuring instrument I developed is applied.

Acknowledgements

I would like to thank my thesis supervisor, Dr. John Milthorpe, for providing sound advice and guidance during my thesis, but also for taking a genuine interest in my chosen topic. I would also like to thank Mr. Andrew Roberts and Mr. Wayne Jealous, who provided exceptional technical support throughout the duration of my thesis. I would like to express my gratitude towards Mr. Chris Edwards who devoted much of his time to building the home-made rocket motors used in this thesis. Thanks go to those of my classmates who made my time at ADFA an enjoyable experience. I am very grateful for the support and motivation my family extended to me over the four years of my Bachelor in Engineering (Aeronautical) degree at the UNSW@ADFA. Being able to spend time with you at home in Buninyong during the University breaks was very rejuvenating. Finally, a very special thank you goes to Ms. Adele Polson who provided unwavering care and support to me during the busy stages of this thesis project. You also enabled me to relax and enjoy myself while spending time with you over the years which enabled me to refocus on my degree studies when it was required.

References

ALLSTAR Network, "Practical Rocketry," *Google Search*, URL: http://www.allstar.fiu.edu/aerojava/rocket2.htm [viewed 27 April 2008].

Anderson, Jr., J. D., *Fundamentals of Aerodynamics*, 4th ed., McGraw-Hill Series in Aeronautical and Aerospace Engineering, Maryland, USA, 2007.

Ashcroft, F., *Life at the Extremes*, Flamingo Publishers, 2001.

Australian Government Department of Defence, *Google Search*, URL: http://www.defence.gov.au/ [viewed 29 September 2008].

Beer, F. P., Johnston, Jr., E. R. & DeWolf, J, T, *Mechanics of Materials*, 4th ed. In SI Units, McGraw-Hill, Singapore, 2006.

Boston, D. W., *Material Safety Data Sheet (MSDS-BP)*, Owen Compliance Services, Inc., Issued 12 Aug 1993, Revised 12 Dec 2005.

Dally, J. W., Riley, W. F. & McConnell, K. G., *Instrumentation for Engineering Measurements*, 2nd ed., John Wiley & Sons, Inc., New York, 1993, Chaps. 1, 7-9.

Estes Industries, *2006 Estes Catalogue*, Estes-Cox Corp., Penrose, USA, 2005.

Estes Industries, *Model Rocket Engine and Igniter Instructions*, Estes-Cox Corp., Penrose, USA, 2001-2003.

Fordham, S., *High Explosives and Propellants*, 2nd ed., Pergamon Press, Oxford, UK, 1980, Chaps. 16-19.

Fuchs, M. D., Peretz, A. & Timnat, Y. M., "Parametric Study of Acceleration Effects on Burning Rates of Metallized Solid-Propellants," *Journal of Spacecraft and Rockets*, Vol. 19, Issue 6, 1982, pp. 539-544.

Heath, M. T. & Dick, W. A., "Virtual Prototyping of Solid Propellant Rockets," *Computing in Science & Engineering*, Vol. 2, Issue 2, March-April 2000, pp. 21-32, IEEE.

Hibbeler, R. C., *Mechanics of Materials*, 2nd ed., Pearson Prentice Hall, New York, 2005.

Hibbeler, R. C., *Engineering Mechanics — Dynamics (SI Edition)*, 2nd ed., Prentice Hall, Singapore, 2002.

Incropera, F. P., DeWitt, D. P., Bergman, T. L. & Lavine, A. S., *Fundamentals of Heat and Mass Transfer*, 6th ed., John Wiley & Sons, MA, USA, 2007.

Inman, D. J., *Engineering Vibrations*, 2nd ed., Prentice Hall, New Jersey, 2001, Chap. 1.

Jensen, G. E. & Netzer, D. W., *Tactical Missiles Propulsion*, Volume 170, Progress in Astronautics and Aeronautics, AIAA, Inc., Massachusetts, USA, 1996.

Kentgens, H., Mackowiak, H. P. & Schoffl, R., "Short-Action Solid Motors with Double-Base Propellants," *Journal of Propellants, Explosives, Pyrotechnics*, Vol. 21, 1996, pp. 118-128.

Kuo, K. K. & Coates, G. R., "Review of Dynamic Burning of Solid Propellants in Gun and Rocket Propulsion Systems," *Symposium (International) on Combustion*, Vol. 16, Issue 1, 1977, pp. 1177-1192, ScienceDirect database.

Moran, M. J. & Shapiro, H. N., *Fundamentals of Engineering Thermodynamics*, 5th ed., John Wiley & Sons, Inc., MA, USA, 2004.

Mungas, G. S., Das, D. K. & Kulkarni, D., "Design, construction and testing of a low-cost hybrid rocket motor," *Aircraft Engineering and Aerospace Technology*, Vol. 75, Issue 3, 2003 Research paper, Emerald.

Munson, B. R., Young, D.F. & Okiishi, T. H., *Fundamentals of Fluid Mechanics*, 5th ed., John Wiley & Sons Inc., USA, 2006.

Nakka, R., "Richard Nakka's Experimental Rocketry Website," *Google Search*, URL: http://www.nakka-rocketry.net/ [viewed 21 March 2008].

Paz, M. & Leigh, W., "Structural Dynamics: Theory and Computation," *Google Books*, 5th ed., Kluwer Academic Publishers, 2004.

Rochford, E. E., "Temperature Sensitivity Measurements of Solid Rocket Propellants," MSc (Engineering) Dissertation, Department of Mechanical and Aerospace Engineering, School of Graduate Studies, University of Alabama, Alabama, USA, 1999.

Rossi, C., Orieux, S., Larangot, B., Do Conto, T. & Esteve, D., "Design, fabrication and modeling of solid propellant micro-rocket application to micropropulsion," *Sensors and Actuators*, A 99, 2002, pp. 125-133, Elsevier Science.

School of Aeronautics and Astronautics, Purdue University, "Solid Rocket Propulsion," *Google Search*, URL: https://engineering.purdue.edu/AAE/Research/Propulsion/Info/rockets/solids/ [viewed 27 April 2008].

Sleeter, D. G., *Amateur Rocket Motor Construction*, The Teleflite Corporation, Moreno Valley, CA, 2004.

Spiegel, M. R. & Liu, J., *Mathematical Handbook of Formulas and Tables*, 2nd ed., Schaum's Outline Series, McGraw-Hill, Singapore, 1999.

Sutton, G. P. & Biblarz, O., *Rocket Propulsion Elements*, 7th ed., John Wiley & Sons, Inc., New York, 2001.

Texnet, "Motor Test Stand," *Google Search*, URL: http://www.texnet.net/ccent/rockets/TestStand/TestStand.htm [viewed 20 March 2008].

Tse, F. S. & Morse, I. E., *Measurement and Instrumentation in Engineering – Principles and Basic Laboratory Experiments*, Marcel Dekker, Inc., New York and Basel, 1989, Chaps. 1-2, 7.

Zaehringer, A. J., *Solid Propellant Rockets – An Introductory Handbook*, American Rocket Co., Wyandotte, Michigan, USA, 1955, Chaps. 2, 5-6.

Zondlo, J. W. & Velez, M. R., "Development of surface area and pore structure for activation of anthracite coal", *Fuel Processing Technology*, Volume 88 Issue 4, 2007, pp. 369-374, Elsevier, Science Direct Database, UNSW Library website.